Journal of Engineering Mathematics **30:** 35–78, 1996.

Helical distributions of stokeslets

SIR JAMES LIGHTHILL
Department of Mathematics, University College London, Gower Street, London, WC1E 6BT, United Kingdom

Received 9 March 1995

Abstract. Helical distributions of stokeslets can valuably model microbial locomotion through a fluid, and also the flow field generated, wherever a flagellum actively executes helical undulations (as in many single-celled algae and protozoa) or where (as in many bacteria) the action of rotary motors causes a passive structure of helical shape (which may be a flagellum or else the cell body itself) to rotate. Here, previous biomechanical studies of such modes of locomotion are extended to include analyses of three-dimensional flow fields. In some cases, a rotlet field (curl of a stokeslet) needs to be incorporated in the models. For example, spirochete swimming is modelled by combined helical distributions of stokeslets and rotlets; the computed flow field being confined to within distances of less than twice the radius of the cell body's helical shape from its axis, while including a powerful jet-like interior flow through the coils of the swimming spirochete.

1. Introduction

A helix is a three-dimensional shape invariant under screw-like combinations of a rotation about its axis and a proportional translation along its axis. A helical distribution of stokeslets, having strengths that are similarly invariant, yields a three-dimensional flow field whose distribution in any plane perpendicular to the axis is repeated in every parallel plane after such rotation and translation. The interesting characteristics of that flow field are the subject of this paper.

Microbiology offers many compelling motivations – as expounded in my 1975 John von Neumann Lecture [1] – for investigating helical distributions of stokeslets. However, a study aimed at microbiological applications can become excessively concentrated on overall characteristics of clear importance to microbiology such as energy dissipation rate, torque and swimming speed and their relationships to the geometry and kinematics of the helix. Those relationships, which I comprehensively probed in [1], are here complemented (Section 2) with a detailed look at the flow field as a whole – after which the paper is continued with outlines of the relevance of these investigations to the locomotion of eukaryotic microorganisms (algae and protozoa; see Section 3) and of bacteria (Section 4), and concluded with a particularly interesting application to the flow field around a spirochete (Section 5). First of all, however, some preliminary microbiological background may perhaps be given very briefly.

The flagellum in a eukaryotic microorganism is a complicated structure capable (Section 3) of generating patterns of bending movements through active sliding of internal tubules relative to one another. These sliding processes are somewhat similar to those involved in the relative motions of adjacent muscle fibrils, and are powered like them by the dephosphorylation of adenosine triphosphate (ATP). In every flagellum the active element, called axoneme, possesses an essentially identical "9 + 2" structure, comprising 9 "doublet" tubules arranged in a circle of diameter 0.2 μm around 2 central tubules. A flagellar membrane surrounds the axoneme; while, in certain species, surrounding additionally an "intraflagellar rod".

Among different single-celled organisms that use such a flagellum (or sometimes two flagella) for propulsive purposes, a diverse range of patterns of bends are so generated in the flagella [1]. Rather prominent among these is the undular pattern, in which a wave is propagated either from the flagellum's base (where it is attached to the cell body) to its tip, or else from tip to base. Waves of both planar and helical forms are found; here, before concentrating on the latter, I offer first a brief overview of planar waves.

It was G.I. Taylor [2-4] who first highlighted the key property of planar wave propagation for flagellar hydrodynamics. This is concerned with movements of any short stretch S of the flagellum relative to the cell body. He pointed out that, although

(i) the average of those movements is zero, nevertheless
(ii) movements of S normal to itself have positive components in the direction of propagation – implying that
(iii) movements tangential to S have, on the average, equal and opposite negative components.

Taylor showed moreover that movements of S normal to itself exert on the fluid a greater force per unit velocity of movement than do tangential movements; therefore, by (ii) and (iii) above, propagation of a wave along the flagellum exerts always a net force on the fluid in the direction of propagation. The reaction of the fluid on the flagellum is then a thrust in a direction opposite to that of the wave propagation; therefore, the whole organism proceeds in this direction at such a speed that its drag balances that thrust. (For a careful discussion of how the force-coefficient approach pioneered by Taylor is related to approaches using stokeslet distributions, see Section 2.3 of my survey [1].)

All these remarks apply to flagella with their active element (the axoneme) surrounded by a smooth flagellar membrane. The soundness of the argument is demonstrated, on the other hand, by a group of microorganisms that exhibit diametrically opposite properties, owing to the presence on the membrane of stiff "hairs" known as mastigonemes which are arranged along opposite sides of the flagellum and project normally to it in the plane of its undulations. Taylor pointed out that these generate a large increase in the force per unit velocity exerted by tangential movements, raising its value above that for normal movements (which the presence of the mastigonemes hardly affects). Therefore, by (ii) and (iii) above, propagation of a wave exerts on the fluid a net force opposite to the direction of propagation; the balancing thrust, therefore, being in the direction of propagation. For example, the chrysophycean alga *Ochromonas* is pulled forwards by the base-to-tip undulation of a flagellum with such mastigonemes which stretches ahead of it; however, no further reference is here made to such organisms because flagella with mastigonemes are used in exclusively planar, rather than helical, undulations.

The one obviously disadvantageous feature of planar undulations for propulsion by smooth flagella is that, although all the movements (ii) of a stretch S of flagellum normal to itself have positive – or, more strictly, nonnegative – components in the direction of propagation, those components are small wherever the flagellum is inclined to this direction at a small angle; while, moreover, they fall to zero twice per wavelength. At each instant, therefore, only part of the flagellar movement produces positive thrust even though the whole is generating viscous energy dissipation. Advantages from avoiding this evident source of reduction in propulsive efficiency may have influenced the evolution of helical undulation – even though (see below) it potentially exhibits a disadvantage of its own.

An axoneme able to execute planar undulations is evidently fitted also for executing a helical undulation, which results (Section 2) from the combination of two planar undulations

in mutually orthogonal planes, with a phase difference of 90° between them. From some points of view, moreover, a helical undulation is even simpler because it involves a straightforward rotation in the pattern of relative sliding movements between adjacent tubules (Section 3).

From the hydrodynamic standpoint, too, a special simplification arises: every short stretch S of flagellum exhibits movements normal to itself with one and the same positive component (ii) in the direction of propagation, while simultaneously its movements tangential to S have equal and opposite negative components (iii). It means that all stretches of flagellum make the same positive contribution to thrust (with, again, all necessarily contributing to viscous energy dissipation), which seems at first sight to ensure maximum propulsive efficiency.

Yet, potentially, there remains one serious disadvantage to propulsion by helical undulation. The forces with which all the different short stretches S of flagellum act on the fluid generate not only a resultant force in the direction of propagation but also a turning moment or torque about that direction. Consequently the reaction of the fluid on the microorganism as a whole includes an opposing torque tending to rotate it at an angular velocity such that this turning moment is itself cancelled by that couple which resists such rotation of the cell body and flagellum combined. Moreover, this turning movement or "corkscrew" rotation is such (Section 2) as to diminish those forces with which the flagellum acts on the fluid; so that the resulting swimming speed is reduced without any diminution of energy dissipation rate. Thus helical undulation, notwithstanding the potential gain in propulsive efficiency (from uniformity of thrust) over planar undulation, poses its own threat to propulsive efficiency (from the corkscrew rotation associated with that turning moment).

In my comprehensive survey of flagellar hydrodynamics [1] I interpreted the observed movements of many organisms with two flagella in terms of the idea that they have evolved so as to realise to the full the efficiency advantage of helical propulsion while avoiding its associated disadvantage. Several examples are described in section 3 below, ranging from cases where the disadvantage is diminished (by passive means, a subsidiary flagellum being used to increase resistance to turning of the organism) through cases where it may be nullified (when two flagella generate equal and opposite torques) to some remarkable cases where the potential disadvantage seems to have been transmuted into an actual advantage!

Yet enough may already have been said here to motivate the study in Section 2 of a particular flow field – the one generated by a helical distribution of stokeslets – which can significantly add to our understanding of how helical undulations of flagella are used in the propulsion of eukaryotic microorganisms. Necessarily, such a flow field may in practice need to be used in a linear combination with other flow fields, as is always possible in flagellar hydrodynamics owing to the linearity of the equations which describe "Stokes flow" (flow at very low Reynolds number). Also, it is essential to use the basic theorem of flagellar hydrodynamics, as described in my earlier paper [5] within this special issue as well as in my John von Neumann Lecture [1], to relate the stokeslet distribution to the actual movements – including forward swimming movements – of the flagellum.

Although the flow analysed in Section 2 is that associated with a helix extending indefinitely in both directions, it may be useful in practice for representing fluid motions in the neighbourhood of a finite flagellum making helical undulations. At the same time, two special features of this flow should be carefully noted:

(a) the derived swimming speed U_o is that obtained from a balance of thrust against the flagellum's own drag, without any allowance for the additional drag of a cell body; while
(b) the torque per unit length which is generated by the helical flagellum gives the fluid motion a vortical character far from the axis of the helix.

Feature (a) implies that no net thrust is exerted by the flagellum, allowing the swimming speed U_o to be designated [1] as the zero-thrust swimming speed. In the presence of a cell body, the swimming speed takes a reduced value U; therefore, relative to its zero-thrust movement, the flagellum is drifting backwards at a velocity $U_o - U$. Thrust consists of the hydrodynamic resistance to that backward drift, and must be balanced against the drag on the cell body moving forward at velocity U. Accordingly, an additional fluid motion, generated by "drag" stokeslets on the cell-body surface opposed by "thrust" stokeslets distributed along the flagellum, needs [1] to be linearly combined with the fluid motion studied in Section 2.

At the same time, feature (b) is itself not fully characteristic of fluid motions far from a real microorganism. As already indicated, various mechanisms act to ensure that the total torque on the whole organism is zero. The most obvious mechanism – rotation of a cell body at an angular velocity Ω determined by the torque applied and its own rotational damping constant – is, actually, allowed for in Section 2, along with the consequent "corkscrew rotation" which it generates. Evidently, at distances comparable with the flagellum's length, the flagellum's far-field vortical motion would be largely cancelled by the far field of motions generated by such cell-body rotation. Alternatively, where two flagella generate equal and opposite helical undulations, the vortical components cancel in the sum of their far fields. For other more complex mechanisms in eukaryotic organisms see Section 3.

Next, some applications of helical distributions of stokeslets to problems of bacterial locomotion are sketched in Section 4. Although the same word "flagellum" is used, not only for the complex structures including actively motile axonemes which contribute to the locomotion of eukaryotic microorganisms, but also for those thin, essentially passive, filamentous structures that confer motility on some bacteria, the differences between them are enormous. The latter, with diameters around 0.02 μm (smaller by an order of magnitude), are driven by a sort of "rotary motor" situated between the outer cell wall and the cytoplasmic membrane. Although in many cases they have helical shapes, these operate in a simple "corkscrew rotation" mode. Both such cases, and some quite different cases where it is the cell body which is helical in shape – being given forward motion through some quite surprising movements of flagella – are described in Section 4 in the context of the general theory of helical distributions of stokeslets. Finally, a flow field of particular interest (that around a swimming spirochete) is given detailed analysis in Section 5, while Section 6 offers a general synopsis of conclusions.

2. The three-dimensional flow field

The propagation of a helical wave along the flagellum of a eukaryotic microorganism can be described [1] by equations

$$y = b\cos[k(s - ct)],\ z = b\sin[k(s - ct)],\ x = \alpha s \tag{1}$$

in terms of the distance s measured along the flagellar centreline; where (for fixed t)

$$\mathrm{d}x^2 + \mathrm{d}y^2 + \mathrm{d}z^2 = \mathrm{d}s^2,\ \text{giving}\ \alpha^2 + b^2k^2 = 1. \tag{2}$$

As remarked in Section 1, the helical wave (1) combines planar undulations in the y- and z-directions with phases differing by 90°.

The wave travels along the curved centreline (1) at velocity c. However, the wave speed V along the x-axis (axis of the helix) is

$$V = \alpha c;\ \text{ while}\ \Lambda = 2\pi/k\ \text{and}\ \lambda = \alpha\Lambda \tag{3}$$

are, respectively, the wavelength Λ measured along the centreline and the "pitch" λ of the helix (wavelength measured along its axis).

The three-dimensional flow field, which depends just on the instantaneous motion of the boundary, is here analysed at time $t = 0$, when the position and velocity of a point (1) on the centreline are

$$(x, y, z) = (\alpha s,\ b\cos ks,\ b\sin ks) \tag{4}$$

and

$$\mathbf{w} = (\dot{x}, \dot{y}, \dot{z}) = (0,\ bkc\sin ks,\ -bkc\cos ks). \tag{5}$$

It is noteworthy that this centreline velocity w is identical with that produced by a simple "corkscrew rotation"

$$\mathbf{w} = (-\omega, 0, 0) \times (x, y, z); \text{ where } \omega = kc \tag{6}$$

is an effective angular velocity of rotation in the negative sense about the x-axis.

On the other hand, any real undulatory movement (1) of a flagellum relative to a cell body may generate movements of the cell body itself. Such movements, of translation and rotation, have to be added on to the velocity (5) if motion of the flagellar centreline relative to the fluid is to be described.

In particular, a wave propagation in the positive x-direction was seen in Section 1 to produce a translational movement in the opposite direction which may be written $(-U, 0, 0)$ in terms of the swimming speed U. At the same time the flagellum's effective rotary movement (6) in the negative sense may be opposed by the fluid with a resistive torque in the positive sense, leading to rotation of the cell body with angular velocity $(\Omega, 0, 0)$. (For some other processes that can influence the value of Ω in certain organisms, see Section 3.)

The case here analysed, as explained in Section 1, is that of a helical flagellum which extends indefinitely in both the positive and negative x-directions. It moves at the "zero-thrust swimming speed"; namely, that speed $U = U_0$ for which the thrust generated by the helical undulation (1) is balanced by the drag opposing movement of the flagellum itself – without any allowance for cell-body drag. Such a condition of zero net thrust permits the three-dimensional flow field to be well defined even around a flagellum of infinite extent (for considerations which determine the value $U < U_0$ of swimming speed when cell-body drag is taken into account, see Section 1). There is however no difficulty in allowing for rotation of the organism as a whole with angular velocity Ω, which reduces the effective angular velocity of the flagellar centreline from its value $\omega = kc$ as in (6) to a value

$$\omega_E = \omega - \Omega. \tag{7}$$

In that case the centreline velocity w is modified from its value (5) to a new value

$$\mathbf{w} = (-U_0,\ \omega_E b\sin ks,\ -\omega_E b\cos ks), \tag{8}$$

which takes into account translation at velocity $(-U_0, 0, 0)$ and rotation with angular velocity $(\Omega, 0, 0)$.

A helical distribution of stokeslets of strength $\mathbf{f}(s)$, representing the force with which unit length of flagellum acts on the fluid, is found [1] to be compatible with the zero-thrust motion (8) if $\mathbf{f}(s)$ takes a form

$$\mathbf{f}(s) = (0,\ h\sin ks,\ -h\cos ks) \tag{9}$$

of similar appearance but with zero x-component; in other words, with no net thrust. The force per unit length (9), when applied at the position (4), generates, however, a net torque $(-bh)$ about the x-axis, equal to the x-component of

$$(\alpha s,\ b\cos ks,\ b\sin ks) \times (0,\ h\sin ks,\ -h\cos ks), \tag{10}$$

per unit length; and it is an equal and opposite reaction of the fluid on unit length of flagellum – namely an opposing couple $(+bh, 0, 0)$ – which may act to determine the organism's rotary movement with angular velocity Ω.

It should also be noted that the rate of working per unit length of flagellum is

$$E = \omega_E bh. \tag{11}$$

This value – the scalar product of the vectors (8) and (9) – can be interpreted as the work being done to rotate the flagellum at the effective angular velocity ω_E against that opposing couple.

I turn now to the three-dimensional flow field generated by a helical distribution of stokeslets of strength $\mathbf{f}(s)$ per unit length. At any field point this takes the form

$$\mathbf{u} = \int_{-\infty}^{\infty} \frac{r_0^2\mathbf{f}(s) + [\mathbf{f}(s)\cdot\mathbf{r}_0]\mathbf{r}_0}{8\pi\mu r_0^3}\mathrm{d}s, \tag{12}$$

where the vector $\mathbf{r}_0$ with magnitude r_0 represents displacement of that field point from the stokeslet location (4). The integral (12), with $\mathbf{f}(s)$ given by (9), converges for all field points except those on the flagellar centreline (where convergence fails because r_0 can become zero).

The exception was already fully treated in [1] by use of the basic theorem of flagellar hydrodynamics [5]. This states that, at each point $s = s_0$ on the centreline, the surface of the flagellar cross-section moves at a velocity $\mathbf{w}(s_0)$ given as the sum of

(a) the integral (12) with the small interval $r_0 < \delta$ excluded (here, $\delta = 0.5e^{1/2}a = 0.824a$ in terms of the flagellar radius a); and

(b) a term proportional to the component $\mathbf{f}_n(s_0)$ of $\mathbf{f}(s_0)$ in a plane normal to the centreline.

That treatment, which determined the relationships between the functions $\mathbf{w}(s)$ and $\mathbf{f}(s)$ given by Eqs. (8) and (9), led to comprehensive data on values of swimming speed, torque and rate of working for given values of a, b, c and k. Here, on the other hand, postponing further reference to exceptional positions of the field point, I analyse "in general" the three-dimensional flow field.

As remarked at the beginning of Section 1, it suffices to determine this in just the plane $x = 0$, intersected by the helix (4) at the point

$$(x, y, z) = (0, b, 0). \tag{13}$$

Indeed, because the helix (4) and the stokeslet distribution (9) are both invariant under a shift of the origin of s to $s = s_0$, along with a translation of the coordinate axes through a distance αs_0 in the x-direction and a rotation through an angle ks_0 about it, the three-dimensional flow field in the plane $x = \alpha s_0$ can be obtained from the flow field in the plane $x = 0$ by a simple rotation through an angle ks_0.

At a general point

$$y = R\cos\phi,\quad z = R\sin\phi \tag{14}$$

in the plane $x = 0$ (where the exceptional point (13) is excluded by avoiding the combination of values $R = b, \phi = 0$) the vector separation $\mathbf{r}_0$ from the stokeslet location (4) takes the form

$$\mathbf{r}_0 = (-\alpha s,\ R\cos\phi - b\cos ks,\ R\sin\phi - b\sin ks), \tag{15}$$

so that the square of its magnitude is

$$r_0^2 = \alpha^2 s^2 + R^2 - 2Rb\cos(ks - \phi) + b^2. \tag{16}$$

Then Eq. (12), with $\mathbf{f}(s)$ given by (9), becomes

$$\frac{8\pi\mu\mathbf{u}}{h} = \int_{-\infty}^{\infty} \frac{(0, \sin ks, -\cos ks)}{r_0}\mathrm{d}s + \int_{-\infty}^{\infty} \frac{R\sin(ks-\phi)\mathbf{r}_0}{r_0^3}\mathrm{d}s, \tag{17}$$

where the second integral is absolutely convergent. Moreover an integration by parts turns the first integral, which converges although not absolutely, into a new form

$$-\int_{-\infty}^{\infty} \frac{(0, \cos ks, \sin ks)}{r_0^3 k}[\alpha^2 s + Rbk\sin(ks-\phi)]\mathrm{d}s \tag{18}$$

with the absolute convergence that is convenient for computational purposes. This gives

$$\begin{aligned}\frac{8\pi\mu\mathbf{u}}{h} &= \int_{-\infty}^{\infty}\Bigg[R\sin(ks-\phi)(-\alpha s,\ R\cos\phi - 2b\cos ks,\ R\sin\phi - 2b\sin ks) \\ &\qquad -\frac{\alpha^2 s}{k}(0,\ \cos ks,\ \sin ks)\Bigg]\frac{\mathrm{d}s}{r_0^3} \\ &= \int_{-\infty}^{\infty} \frac{X\sin(\theta-\phi)[-\alpha\beta\theta,\ \beta^2(X\cos\phi - 2\cos\theta),\ \beta^2(X\sin\phi - 2\sin\theta)] - \alpha^2\theta(0, \cos\theta, \sin\theta)}{[\alpha^2\theta^2 + \beta^2(X^2 - 2X\cos(\theta-\phi) + 1)]^{3/2}}\,\mathrm{d}\theta,\end{aligned} \tag{19}$$

where the substitution $ks = \theta$ has been made along with introduction of the nondimensional quantities

$$R/b = X \text{ and } bk = \beta;\ \text{so that, by Eq. (2), } \alpha^2 + \beta^2 = 1. \tag{20}$$

Before investigating the three components of expression (19) when X and ϕ take general values, I focus first on the case $\phi = 0$ which includes the exceptional values $X = 1,\ \phi = 0$ already treated in [1]. When $\phi = 0$, the integrand's denominator is an even function of θ, allowing the integral to be simplified by combining values of the integrand for θ and -θ to give

$$\frac{4\pi\mu\mathbf{u}}{h} = -[\alpha\beta X B_1(\alpha, X),\ 0,\ 2\beta^2 X B_2(\alpha, X) + \alpha^2 B_1(\alpha, X)], \tag{21}$$

where for general X the functions $B_1,\ B_2$ are defined as

$$\{B_1(\alpha, X),\ B_2(\alpha, X)\} = \int_0^{\infty} \frac{\{\theta\sin\theta,\ \sin^2\theta\}}{[\alpha^2\theta + \beta^2(X^2 - 2X\cos\theta + 1)]^{3/2}}\mathrm{d}\theta. \tag{22}$$

It is only in the exceptional case $X = 1$ that the integrals (22) fail to converge, with both integrands behaving (since $\alpha^2 + \beta^2 = 1$) like θ^{-1}as $\theta \to 0$. In that exceptional case

the range of integration has the small interval $0 < \theta < \epsilon$ excluded (see (a) above; here, $\epsilon = k\delta = 5.2a/\Lambda$) and functions $A_1(\alpha)$ and $A_2(\alpha)$ have been defined [1] so that

$$\{-\ln\epsilon + A_1(\alpha),\ -\ln\epsilon + A_2(\alpha)\} = \int_\epsilon^\infty \frac{\{\theta\sin\theta,\ \sin^2\theta\}}{[\alpha^2\theta^2 + 2\beta^2(1-\cos\theta)]^{3/2}}\mathrm{d}\theta \tag{23}$$

for small ϵ. Then, in order to obtain the velocity w on the surface of the flagellar cross-section $s = 0$, Eq. (21) has to be used for $X = 1$ with these expressions (23) replacing $\{B_1,\ B_2\}$ and with an addition of two terms: the extra term

$$\alpha(\beta, 0, -\alpha) \tag{24}$$

proportional (see (b) above) to the component of stokeslet strength normal to the flagellar centreline, and another extra term

$$\tfrac{1}{2}\left[\frac{(0,\ \cos ks,\ \sin ks}{r_0 k}\right]_{-\delta}^{\delta} = (0,0,1) \tag{25}$$

which emerges from the integration by parts applied to the first integral in (17) when the interval $|s| = r_0 < \delta$ is excluded from this integral. Then a comparison with the value of w for $s = 0$ specified by Eq. (8) gives the results

$$\left.\begin{aligned} 4\pi\mu U_0/h &= \alpha\beta(-\ln\epsilon + A_1 - 1), \\ 4\pi\mu\omega_E b/h &= 2\beta^2(-\ln\epsilon + A_2) + \alpha^2(-\ln\epsilon + A_1 + 1) - 1 \end{aligned}\right\}. \tag{26}$$

These results (26), numbered as Eqs. (56) in [1], were comprehensively applied there (after the functions $A_1(\alpha)$ and $A_2(\alpha)$, as defined above in Eqs. (23), had been plotted in Fig. 11) to derive, and to exhibit in Fig. 12, several key conclusions on zero-thrust swimming by helical flagella. Here, that Fig. 12 from [1] is reproduced with a new caption as Fig. 1; from which various inferences regarding the locomotion of microorganisms are drawn in Sections 3 and 4 below.

But I concentrate first on the shapes of the lower curves, which show how the ratio $E/\mu U_0^2$ – a nondimensional measure of the flagellar rate of working E (per unit length) against viscous dissipation at swimming speed U_0– varies with α for different flagellar wavelength-to-radius ratios Λ/a. In every case, a minimum rate of working for given swimming speed is approximately achieved when

$$\alpha^2 = \beta^2 = 0.5, \tag{27}$$

a geometrical configuration actually depicted in the bottom right-hand corner of Fig. 1. Because this configuration, which appears to offer locomotion at minimum power consumption, is also typical of observed flagellar undulations , I use it in the following analyses of the three-dimensional flow field.

Fig. 2 plots the functions $B_1(\alpha, X)$ and $B_2(\alpha, X)$ for $X > 0$ in this case (27). At the exceptional point $X = 1$ where B_1 and B_2 become logarithmically infinite, those values (23) which need to be used there are inserted for a typical wavelength-to-radius ratio $\Lambda/a = 100$ (which gives $\ln\epsilon = -2.96$). For every negative X, on the other hand, the integral expressions (22) for B_1 and B_2 converge and are also plotted in Fig. 2. These are of interest because for $\phi = \pi$, as is easily verified, the three-dimensional flow field (19) is given by Eq. (21) after the substitution of $(-X)$ for X.

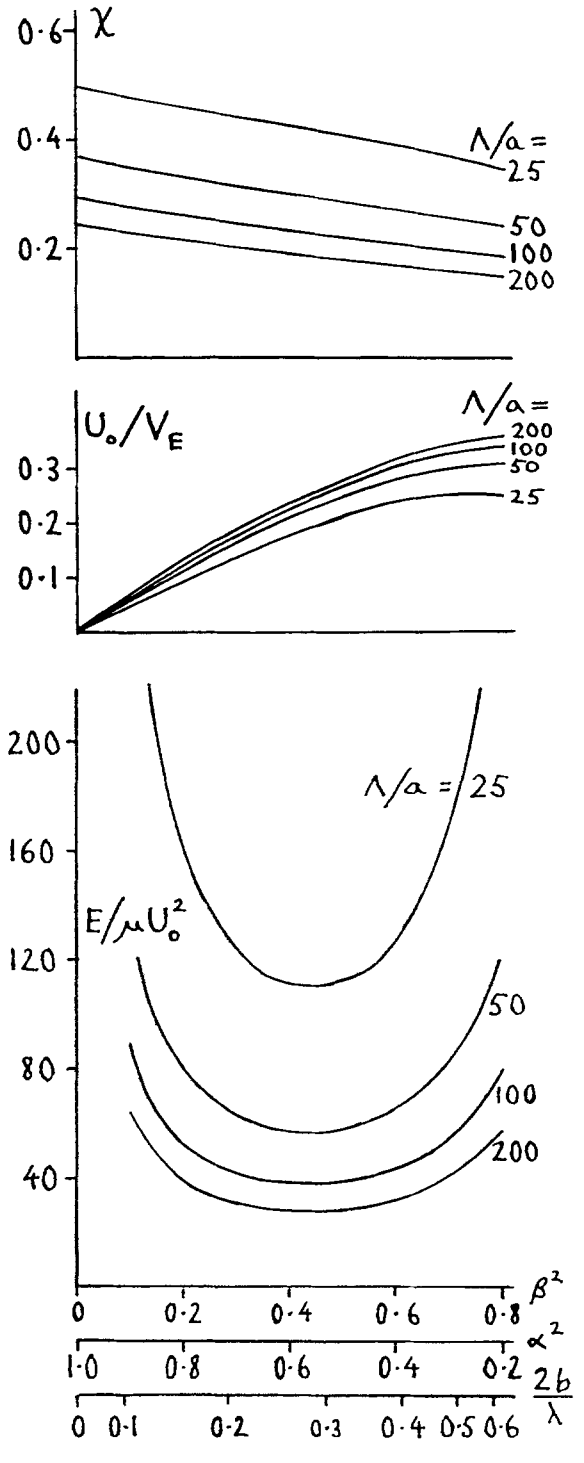

Ratio $X = \dfrac{\text{torque per unit length}}{4\pi\mu b^2 \omega_E}$

(μ = viscosity of fluid, ω_E = effective angular velocity of helix).

Ratio U_0/V_E (U_0 = swimming speed, $V_E = \dfrac{\alpha\omega_E}{k} = \lambda\dfrac{\omega_E}{2\pi}$ = effective wave speed).

Ratio $E/\mu U_0^2$ (E = energy dissipation per unit length).

Geometry of helix: $\beta = bk$, $\beta^2 = 1 - \alpha^2$, where α = axial direction cosine, b = radius of helix; $k = 2\pi/\Lambda$, where Λ = wavelength as measured along helix, $\lambda = \alpha\Lambda$ = wavelength measured along axis.

Fig. 1. Biomechanical conclusions on zero-thrust swimming by a helical shape with circular cross-sections of radius a. Here, the effective angular velocity ω_E takes the form $\omega - \Omega$ which allows for the whole organism's response (a counter-rotation at angular velocity Ω) to the resistive torque bh per unit length. The same horizontal scale (shown in three versions) applies to the torque, swimming speed and energy dissipation diagrams. Energy dissipation E per unit length of flagellum is a minimum in conditions (around $\alpha^2 = \beta^2 = 0.5$) for which the aspect-ratio $2b/\lambda$ of the helix takes the value 0.3 used for illustration in the right-hand diagram. Fig. 1 is based on the same data as Fig. 12 of [1] (where, however, labels on U_0/V_E curves were misprinted in reverse order) but includes results for $\Lambda/a = 25$ which are found relevant to motions of the bacterium *Spirillum* (Section 4) while omitting those for $\Lambda/a = 400$ which seem to lack microbiological relevance.

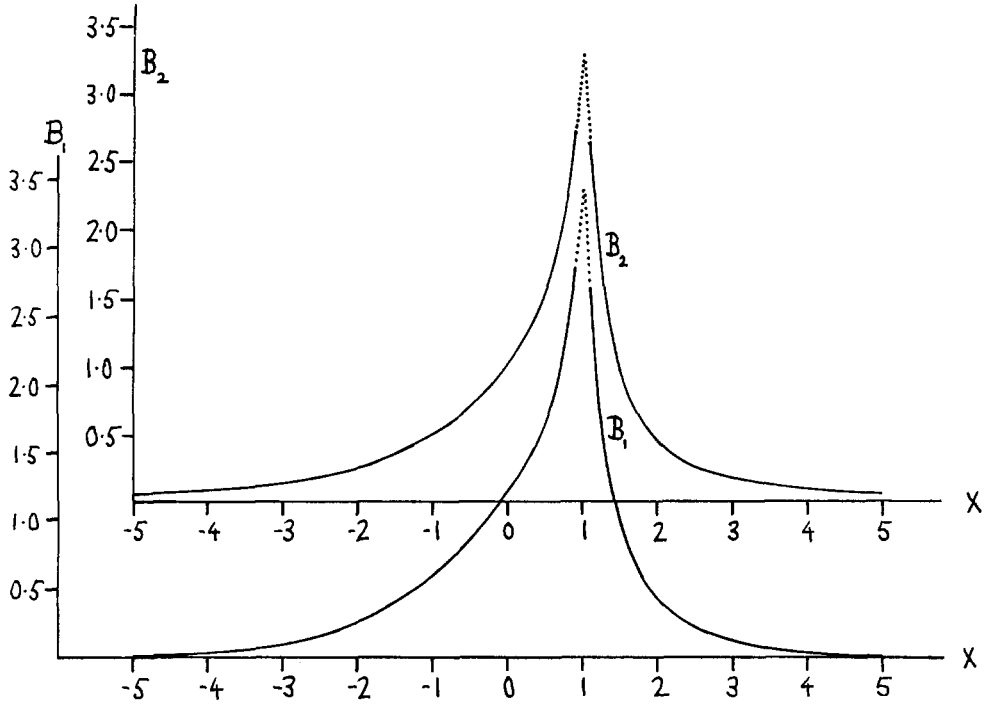

Fig. 2. Here, the functions (22) are plotted (solid lines) for all values of X except those near $X = 1$, where dotted lines indicate a transition to the limiting values (23) computed for $\Lambda/a = 100$.

It may be noted that, for large $|X|$, the function B_1 tends exponentially to zero like a multiple of the Bessel function $K_0(|X|)$, whereas B_2 becomes algebraically small like a multiple of X^{-2}. This latter function appears just in the z-component of (21), which it causes to fall off like X^{-1} in the expected vortex-type far field.

These distinctions become even clearer in Figs. 3 and 4, depicting fluid velocity components in the x-direction (along the axis of the helix) as well as in planes at right angles to it. In Fig. 3 the solid line shows the x-component of expression (21) for $4\pi\mu u/h$, which, once again, falls off exponentially for large $|X|$. It may also be noted that its limiting value as $X \to 1$ does not precisely depend on a replacement of expressions (22) by (23), because of the need to incorporate the extra term (24); thus, the solid line represents $-\alpha\beta X B_1$ for general X but for $X = 1$ takes the value $-\alpha\beta(-\ln\epsilon + A_1 - 1)$ as in Eqs. (26).

A striking feature of Fig. 3 is that the solid line exhibits for $X > 0$ the expected negative axial velocities, associated with swimming movements in directions opposite to that of wave propagation; but that, in stark contrast, there is flow in the positive x-direction (backflow) for $X < 0$. As already mentioned this corresponds to motions of fluid where $\phi = \pi$. Also, a computation of the x-component of $4\pi\mu u/h$ for $\phi = \pi/2$ and $\phi = -\pi/2$ (easy because the integral (19) in these cases offers no convergence problems) again yields positive values – given by the broken line in Fig. 3.

Moreover, no exhaustive computing is needed to see that, for general values of X, negative and positive values of the axial velocity are in exact balance – in the sense that their ϕ-average is zero. In fact, the integral with respect to ϕ of the x-component of (19) from $\phi = -\pi$ to

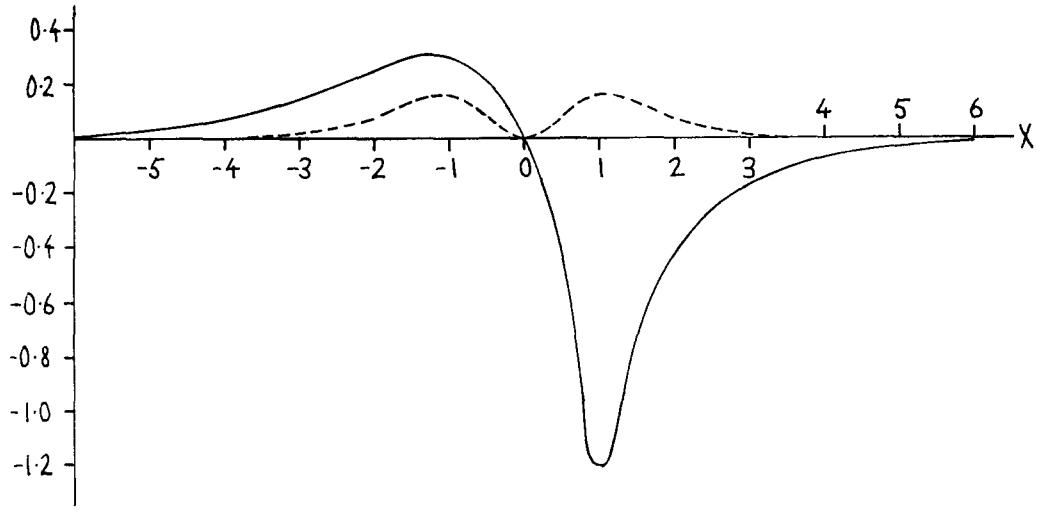

Fig. 3. Illustrating axial motions of fluid (x-components of $4\pi\mu\mathbf{u}/h$), computed for $\alpha^2 = \beta^2 = 0.5$ in the plane $x = 0$ intersected by the helix at the point $y = b$, $z = 0$. Because a change by $\pm\pi$ in the polar angle ϕ has the same effect on the velocity field (19) as a sign change for $X = R/b$, the solid line (computed for $\phi = 0$ and real X) gives values on the y-axis with $X = y/b$ while the broken line ($\phi = \pi/2$) gives values on the z-axis with $X = z/b$. Axial velocities which are negative (that is, in the direction of swimming) are precisely balanced by "backflow" in the positive x-direction, as indicated by Eq. (28).

$\phi = \pi$ vanishes; simply because

$$\int_{-\pi}^{\pi} \frac{X\sin(\theta-\phi)\mathrm{d}\phi}{[\alpha^2\theta^2+\beta^2(X^2-2X\cos(\theta-\phi)+1)]^{3/2}} = -\frac{1}{\beta^2}\left[\frac{1}{[\alpha^2\theta^2+\beta^2(X^2-2X\cos(\theta-\phi)+1)]^{1/2}}\right]_{-\pi}^{\pi} \tag{28}$$

is zero (the integrated term takes the same value at both limits).

A helical distribution of stokeslets produces, then, axial velocities that are highly localised. They fall off exponentially with distance from the axis; furthermore, at every such distance, the negative axial velocities near the helix are balanced (in the sense of an average with respect to ϕ) by positive "backflow" velocities.

By contrast, the velocity components in a plane perpendicular to the axis of the helix are shown in Fig. 4 to be far from localised. Indeed, because the fluid is subjected to a torque $(-bh)$ per unit length of flagellum about the x-axis – which amounts to a torque $(-bh/\alpha,\ 0,\ 0)$ per unit distance along that axis, a vortical far field

$$\mathbf{u} = \left(0,\ \frac{bh}{\alpha}\frac{\sin\phi}{4\pi\mu R},\ -\frac{bh}{\alpha}\frac{\cos\phi}{4\pi\mu R}\right) \tag{29}$$

is generated. In nondimensional terms this gives, for large X,

$$\frac{4\pi\mu\mathbf{u}}{h} = \left(0,\ \frac{\sin\phi}{\alpha X},\ -\frac{\cos\phi}{\alpha X}\right). \tag{30}$$

In Fig. 4, curve (a) plots the exact values of the z-component of expression (21) for $4\pi\mu\mathbf{u}/h$ where $\phi = 0$ (values for positive X) and where $\phi = \pi$(values for negative X). They coincide

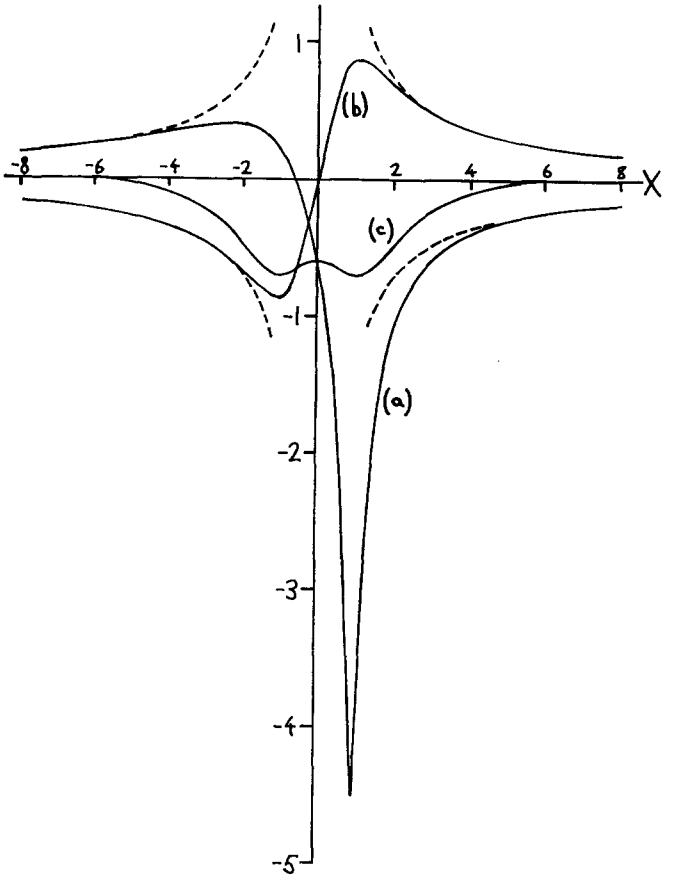

Fig. 4. Illustrating fluid motions at right angles to the axis of the helix. The solid lines give computed components of $4\pi\mu\mathbf{u}/h$ as follows: (a) its z-component on the y-axis (where however the y-component vanishes) with $X = y/b$, alongside (b) its y-component and (c) its z-component on the z-axis, both with $X = z/b$. The broken lines show the vortical far-field forms (30) to which curves (a) and (b) are asymptotic.

with those given – see broken line – by Eq. (30) for $|X| > 5$. Once again, the value at the exceptional point $X = 1$ of this z-component of $4\pi\mu\mathbf{u}/h$ has been included for $\Lambda/a = 100$ as given by the basic theorem of flagellar hydrodynamics (in (26), it is minus the right-hand side of the second equation).

Such a vortical interpretation is further reinforced by a study of curve (b), which plots the y-component of $4\pi\mu\mathbf{u}/h$ where $\phi = \pi/2$ (values for positive X) and where $\phi = -\pi/2$ (values for negative X). Once again, the broken lines indicate values given by Eq. (30); which, this time, have already begun to coincide with curve (b) for $|X| > 2.5$. Yet curve (c), in another striking contrast, plots the z-component of $4\pi\mu\mathbf{u}/h$ for $\phi = \pm\pi/2$; which are values of ϕ for which the z-component of the vortical far field (30) is zero. This is why curve (c) depicts much more localised motions which (just as in Fig. 3) fall off exponentially for large $|X|$.

A geometrically much clearer feel for the distribution of velocity components in the plane $x = 0$ (at right angles to the axis of the helix) is obtained when the data of Fig. 4 are replotted as in Fig. 5. This shows the velocity vector at points $y = 0.4bN$, $z = 0$ (where N takes integer values from -20 to $+20$; thus, the actual position $y = b$, $z = 0$ of the helix itself is

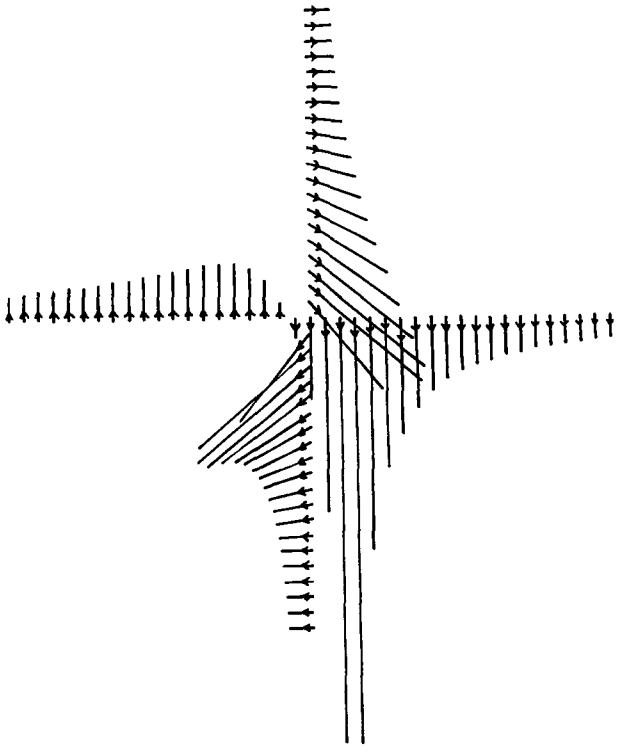

Fig. 5. Here the data of Fig. 4 are replotted as vectors representing values on the y-axis and on the z-axis of fluid velocities resolved onto the (y, z) plane $x = 0$.

omitted) as derived from curve (a), and also the velocity vector at points $y = 0,\ z = 0.4bN$ (for the same range of N) as derived from curves (b) and (c). Each vector represents the velocity resolved onto the plane $x = 0$ (for x-components see Fig. 3) with its length giving the magnitude of that resultant (on the scale indicated in Fig. 4) and the arrow giving its direction.

This pattern of velocity vectors in Fig. 5 shows the salient features of the flow field in the y, z plane very clearly. Near the helix itself ($y = b,\ z = 0$) which, per unit length, exerts in the negative z-direction a force $(0, 0, -h)$, strong velocity components in the negative z-direction are induced (even on the z-axis itself). At rather greater distances, on the other hand, these become overshadowed by the collective effect of the average torque per unit length generated all along the helix.

Against the background of this physical interpretation of y- and z-components of the flow field in the plane $x = 0$ it is worth reconsidering the earlier results on x-components (Fig. 3) with the aim of asking at the conclusion of Section 2 if they can be given any analogous interpretation. Any such enquiry must, of course, begin by acknowledging its greater difficulty, resulting from the fact that x-components of flow in the plane $x = 0$ cannot be influenced by the action of a stokeslet which actually lies in that plane. Thus any attempt at a physical interpretation of those x-components of flow must relate them to the effect of stokeslets in nearby planes with either positive or negative s.

In Fig. 6, showing the positions and orientations of stokeslets for a positive and a negative value of s (each with the magnitude of ks moderately small), the two lines L_+ and L_- are straight lines passing through the origin and one or other of the stokeslets. In the associated

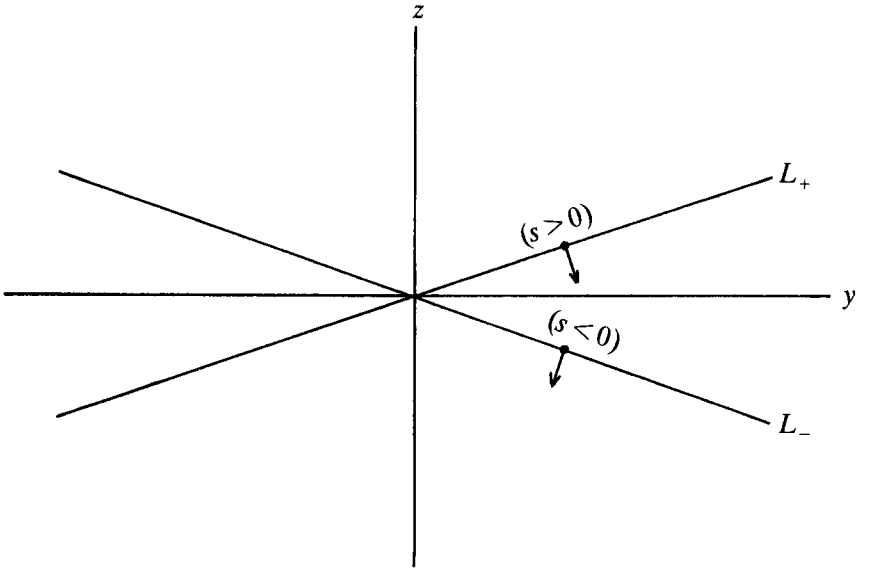

Fig. 6. Illustrating, in the (y, z) plane, the positions and orientations of stokeslets for a positive and a negative value of s, both with $|\ ks\ |$ moderately small. In each case the factor in square brackets in Eq. (31) is positive below the radial line (L_+ or L_-) through the stokeslet and negative above it.

stokeslet fields – each expressed by the integrand of Eq. (12) – the first term in the numerator has no x-component, but the second has x-component

$$-\alpha s\,[\mathbf{f}(s)\cdot\mathbf{r}_0] \tag{31}$$

on the plane $x = 0$. Here the factor in square brackets is positive below the associated line (L_+ or L_-) in each case, and negative above it. From this geometrical property of expression (31) three conclusions may be drawn:

(i) the wedge-shaped region that includes the positive y-axis ($\phi = 0$ in polar coordinates) receives negative contributions to the x-component of flow from both nearby stokeslets, because it lies below L_+ where $s > 0$ and also above L_- where $s < 0$;

(ii) conversely, the wedge-shaped region that includes the negative y-axis ($\phi = \pi$) receives positive contributions to the x-component of flow (that is, backflow) from both nearby stokeslets, lying as it does above L_+ where $s > 0$ and below L_- where $s < 0$;

(iii) moreover, in the rest of the plane, where contributions of opposite signs arise from the two stokeslets, the contribution from a nearer stokeslet is likely to be greater (the r_0^{-3} factor in the integrand of (12) being important here); so that positive x-components of flow (backflow) tend to arise not only on the positive z-axis ($\phi = \pi/2$) which lies above the line L_+ associated with the nearer stokeslet with $s > 0$, but also on the negative z-axis ($\phi = -\pi/2$) which lies below the line L_- associated with the stokeslet with $s < 0$ which is nearer in this case.

These considerations, offering some intuitive feel for why, in the distribution of x-velocities, backflow plays such a substantial role, conclude my physical discussion of results on the three-dimensional flow field.

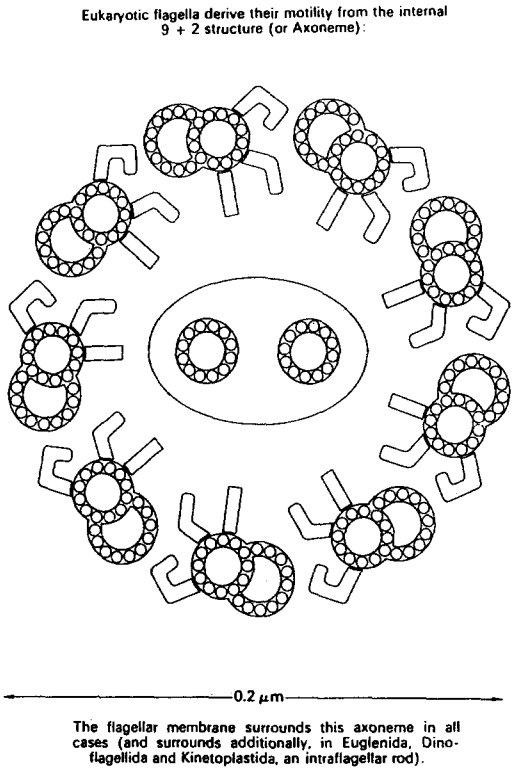

Fig. 7. In eukaryotic microorganisms, each flagellum contains an axoneme whose cross-section takes the form sketched here [1] from comprehensive data in a paper [6] by Warner and Satir. Note those attachments to each doublet tubule which permit active sliding relative to an adjacent tubule.

3. Helical propulsion in eukaryotic microorganisms

In eukaryotic microorganisms the flagellum possesses (see Section 1) an active component, the axoneme, capable of producing bending movements of many kinds. Here I focus on its use for generating helical undulations.

The axoneme consists (Fig. 7, derived from [6]) of 9 tubules of "doublet" form surrounding 2 "singlet" tubules. Each doublet tubule includes attachments which allow it to slide actively relative to the adjacent doublet tubule. This sliding process (see [1] and [6] for more details) involves the breaking of existing chemical bonds between those attachments and the adjacent tubule, followed by the formation of new bonds with molecules further along that tubule. The sliding is powered by the dephosphorylation of adenosine triphosphate (ATP).

In a journal with readers expert in engineering mathematics, I ought perhaps to contrast such a process of bending generated when 9 inextensible tubules slide relative to one another with classical analyses of the bending of an elastic rod. They find that, to a close approximation, plane sections remain plane – so that fibres become extended on the outside of any bend and shortened on the inside. By contrast, active sliding means that plane cross-sections need not remain plane, which can reconcile bending with the inextensibility of each tubule.

Another interesting contrast emerges when we compare the active use of the axoneme to generate helical undulations with an alternative process involving pure corkscrew rotation. Although both processes are shown in Section 2 to produce the same movements of the

centreline (see Eqs. (5) and (6) for these), nevertheless they exhibit important differences in behaviour of each flagellar cross-section relative to its centreline. Specifically, corkscrew rotation necessitates a rotation of the cross-section's whole surface relative to its centreline (as in movements of bacterial flagella discussed in Section 4), whereas helical undulations take place without any such relative rotation.

Just a simple revolving pattern of active sliding between adjacent tubules is required at each cross-section – to be repeated at other sections with a phase lag that of course increases in the direction of propagation – if helical undulation is to be achieved. The following analysis determines this pattern in quantitative detail.

Here, using capital letters to avoid overlap with notation in other sections, I write

$$S = s - ct \text{ so that } \mathbf{C} = (\alpha s,\ b\cos kS,\ b\sin kS) \tag{32}$$

is the centreline locus (1), with unit tangent vector

$$\mathbf{T} = \partial\mathbf{C}/\partial s = (\alpha,\ -\beta\sin kS,\ \beta\cos kS). \tag{33}$$

The effective axoneme radius – that is, the radius from its centre to one of the doublet tubules – is written A, so that a typical location of the core of such a tubule relative to a flagellar centreline stretched straight along the x-axis is

$$A\mathbf{Q},\ \text{where } \mathbf{Q} = (0,\ \cos\psi,\ \sin\psi) \tag{34}$$

is a unit radial vector.

Now I study how this relative position changes in the undulating movement (32), noting first that the component of $\mathbf{Q}$ along the tangent vector (33) is

$$\mathbf{Q}\cdot\mathbf{T} = -\beta\sin(kS - \psi). \tag{35}$$

It follows that the vector $\mathbf{N}$ obtained by resolving $\mathbf{Q}$ onto the plane perpendicular to the tangent $\mathbf{T}$ is

$$\mathbf{N} = \mathbf{Q} - (\mathbf{Q}\cdot\mathbf{T})\mathbf{T} = \mathbf{Q} + \beta\sin(kS - \psi)\mathbf{T}, \tag{36}$$

while the magnitude of $\mathbf{N}$ is found to be

$$N = [1 - \beta^2\sin^2(kS - \psi)]^{1/2}; \tag{37}$$

a value obtained most easily by recalling that the sum of the squares of the resultants of the unit vector $\mathbf{Q}$ in these perpendicular directions must be 1.

In a helical undulation (32), where (see above) the cross-sections themselves are not rotated, a typical location (34) of a tubule core relative to the centreline is mapped onto a position

$$\mathbf{P} = \mathbf{C} + AN^{-1}\mathbf{N} \tag{38}$$

for the same tubule. In other words, its position relative to some centreline point (32) is a product of the effective radius A with a unit vector $N^{-1}\mathbf{N}$ in a direction obtained by resolving $\mathbf{Q}$ onto the plane of a flagellar cross-section. Eq. (38) may be used for the location of each of the nine tubules by giving ψ nine equally spaced values (the spacing being 40°; that is, $2\pi/9$ radians).

I can now verify the impossibility of plane sections remaining plane by calculating how the distance ds_ψ along one of the tubules (38) for a particular value of ψ is related to distance

$\mathrm{d}s$ along the centreline. The rate of change of position $\mathbf{P}$ with s for fixed t is given by (38) and (33) as

$$\partial \mathbf{P}/\partial s = \mathbf{T} + A\partial(N^{-1}\mathbf{N})/\partial s, \tag{39}$$

where the first term has magnitude 1. Also, because the second term includes the factor A (the axoneme radius, very small compared with the flagellar wavelength), it suffices to determine the magnitude of (39) to the first order in A as

$$\mathrm{d}s_\psi/\mathrm{d}s = |\partial P/\partial s| = 1 + A\mathbf{T}\cdot\partial(N^{-1}\mathbf{N})/\partial s, \tag{40}$$

with $\mathbf{N}$ given by Eq. (36).

Three facts can be used to simplify expression (40): $\mathbf{T}$ and $\mathbf{N}$ are orthogonal ($\mathbf{T}\cdot\mathbf{N} = 0$) and $\mathbf{T}$ is of fixed unit magnitude ($\mathbf{T}\cdot\partial\mathbf{T}/\partial s = 0$) while expression (34) for $\mathbf{Q}$ is independent of s. It follows that

$$\mathrm{d}s_\psi/\mathrm{d}s = 1 + AN^{-1}\beta k\cos(kS - \psi), \tag{41}$$

a rather simple expression for the ratio of distance $\mathrm{d}s_\psi$ along a tubule for given ψ to the corresponding centreline distance $\mathrm{d}s$. With expression (37) for N, it can be integrated to give

$$s_\psi = s + A\sin^{-1}[\beta\sin(kS - \psi)]. \tag{42}$$

Eq. (42), with $S = s - ct$ as in (32), not only confirms that tubule inextensibility is incompatible with plane sections remaining plane but also specifies the amount by which this inextensibility requires each tubule to be shifted out of its initial plane during undulation. This shift (in the direction s increasing) is given by the second term on the right-hand side, which may be written

$$AF(ks - \omega t - \psi) \quad \text{with} \quad F(Z) = \sin^{-1}(\beta\sin Z). \tag{43}$$

The necessary pattern of shifts is revolving around the axoneme at angular velocity $\omega = kc$(see (6) above), with different phases ψ for each tubule. The shift relative to an adjacent tubule is

$$AG(ks - \omega t - \psi) \quad \text{with} \quad G(Z) = F(Z) - F(Z - 2\pi/9), \tag{44}$$

of which the time-derivative gives the sliding velocity as

$$-\omega AG'(ks - \omega t - \psi). \tag{45}$$

Fig. 8 shows the periodic functions $G(Z)$ and $G'(Z)$ for the case $\alpha^2 = \frac{1}{2}$ on which I focus in Sections 2 and 3. The simple revolving pattern of sliding (45) is repeated for each value of s with a phase lag which increases in the direction of propagation.

Helical undulation, then, makes no specially complex demands on the organisation of patterns of relative sliding of adjacent tubules in an axoneme. Accordingly, in the remainder of this section, I can concentrate primarily on its advantages and disadvantages in relation to propulsive efficiency.

Its principal advantage, as noted in Section 1, is linked with the uniformity of contributions from all along the flagellum to the rate at which the flagellar movements that yield a given swimming velocity are doing work against viscous dissipation. Such uniformity is beneficial

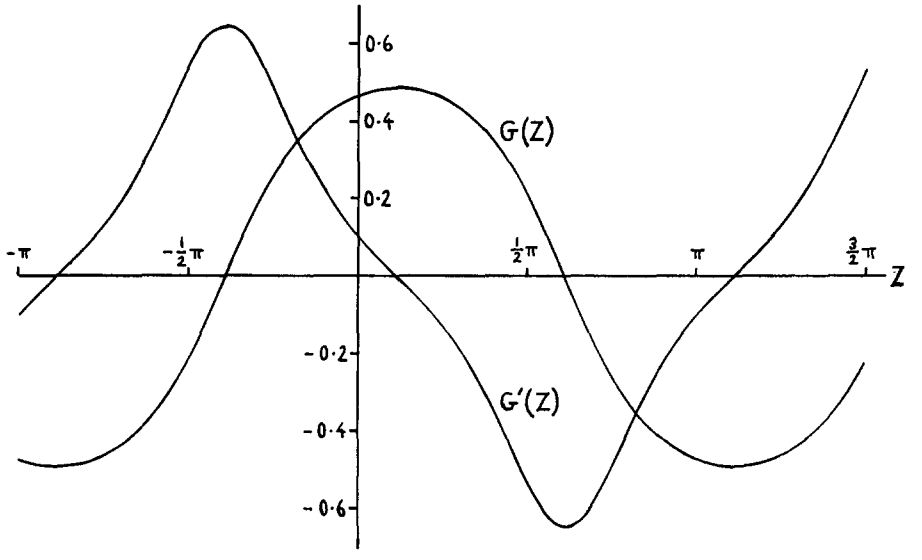

Fig. 8. Illustrating the active sliding movements required for a flagellum to execute helical undulations; these involve displacements of each tubule (relative to the next) described by the function $G(z)$, with sliding velocities described by $G'(Z)$, as in Eqs. (44) and (45).

because swimming velocity is related linearly, whereas rate of working is related quadratically, to flagellar movements – and, broadly speaking, the ratio of the mean square of any quantity to the square of its mean is least when the quantity deviates negligibly from that mean. In the zero-thrust case, moreover, the uniform ratio $E/\mu U_0^2$ is itself minimised under condition (27) with $\alpha^2 = \frac{1}{2}$.

But helical undulation has a counterbalancing disadvantage, also noted in Section 1. It causes the flagellum to be acted on by the fluid with a couple or torque $(bh, 0, 0)$ per unit length (see (10) above), which can determine the angular velocity $(\Omega, 0, 0)$ of a superimposed corkscrew rotation.

Here, I analyse first those relatively simple cases when the torque bhL on a flagellum of total length L is balanced by the couple $D\Omega$ resisting rotation of the cell body at angular velocity Ω (here, D may be described as the cell body's rotational damping constant). In other words, Ω is determined by a balance equation

$$D\Omega = bhL. \tag{46}$$

Moreover, the second of Eqs. (26) allows the torque bh per unit length to be written in terms of χ, the reciprocal of the right-hand side, as

$$bh = 4\pi\mu b^2 \chi \omega_E, \tag{47}$$

with χ plotted in the upper part of Fig. 1. Eqs. (46) and (47) together give an expression

$$\frac{\omega_E}{\omega} = \frac{\omega_E}{\omega_E + \Omega} = \left(1 + \chi \frac{4\pi\mu b^2 L}{D}\right)^{-1} \tag{48}$$

for the factor by which the effective angular velocity ω_E falls short of the angular velocity $\omega = kc$ directly associated with the helical undulation (1).

This reduction factor (48) is important for two reasons. First, the swimming velocity U_0 is diminished by the same factor. Indeed the ratio

$$\frac{kU_0}{\alpha\omega_E}, \text{ equal to } \frac{U_0}{V_E} \text{ with } V_E = \alpha c_E = \alpha\frac{\omega_E}{k}, \tag{49}$$

is fixed by Eqs. (26) as (β/α) times the ratio of their right-hand sides, and this is plotted in the middle part of Fig. 1; for example, it takes the value 0.27 in the case (27) with $\Lambda/a = 100$ on which I focus on this paper. Thus any reduction in ω_E diminishes also U_0. (In expression (49), V_E is the effective wave velocity along the axis of the helix; in other words, the wave's speed relative to the cell body as viewed under a microscope.)

Secondly, propulsive efficiency is diminished by the same reduction factor (48). Thus although it might be supposed that the plot of $E/\mu U_0^2$ in the lower part of Fig. 1 has specified once for all the energy dissipation E per unit length of flagellum for swimming speed U_0, nonetheless an additional rate of energy dissipation $D\Omega^2$ arises from cell body rotation at angular velocity Ω against an opposing torque $D\Omega$. Therefore the total energy dissipation takes the form

$$D\Omega^2 + EL, \tag{50}$$

which Eqs. (46) and (11) allow to be written as

$$\Omega(bhL) + (\omega_E bh)L = \omega bhL = \frac{\omega}{\omega_E}(EL), \tag{51}$$

greater by the factor ω/ω_E than the dissipation due to flagellar movements alone.

Admittedly, this analysis of dissipation has tacitly made an approximation, by assuming that a linear combination of flow fields due to flagellar movements and to cell body rotation produces viscous dissipation equal to the sum of that associated with each flow field separately – even though viscous dissipation has a quadratic dependence on gradients of fluid velocity. Here, however, studies of the former flow field (Section 2 above), combined with results on flows due to body rotation, show their dissipation fields to be spatially separate to such an extent that expression (51) should be quite a close approximation.

Actually, the leading term in the flow field of a rotating body that exerts a torque $(D\Omega, 0, 0)$ on the fluid is the well known "rotlet" field

$$D\Omega\left[\frac{(0, -z, y)}{8\pi\mu r^3}\right], \text{ where } r^2 = x^2 + y^2 + z^2 \tag{52}$$

and the origin is taken at a central point within the body. In (52) the expression in square brackets may be identified with a limit as $\epsilon \to 0$ of four stokeslets of strengths

$$(0, 0, \pm(2\epsilon)^{-1}) \text{ at } (0, \pm\epsilon, 0) \text{ and } (0, \mp(2\epsilon)^{-1}, 0) \text{ at } (0, 0, \pm\epsilon), \tag{53}$$

which evidently represent a set of forces equivalent to a couple of moment $(1, 0, 0)$.

Two considerations suggest that the dissipation fields of this flow (52) and of the flow due to flagellar movements are spatially separated. First of all, the regions of large velocity gradient (leading to large dissipation) within the three-dimensional flow field depicted in Figs. 3,4 and 5 are regions with the distance $R = (y^2 + z^2)^{1/2}$ from the x-axis limited to values between 0 and about $2b$, where b is the radius of the helix; yet their distance x from the cell-body centre is in general much greater, so that the r^3 in the denominator of the rotlet field

(52) makes it small in those regions. Secondly, the distribution of viscous dissipation per unit volume in this field (52) is readily calculated as

$$9\mu\left(\frac{D\Omega}{8\pi\mu}\right)^2\frac{y^2+z^2}{r^8} \tag{54}$$

which – with, now, an r^8 in the denominator – is small for values of x in the region of the flagellum; that is, values of x exceeding its maximum value on the body surface. Indeed, even for a spherical cell body, we may verify that only 1 part in 16 of the total energy dissipation, distributed as in (54), appears in the region with x exceeding the sphere radius (while the fraction may be expected to be even less for more elongated bodies).

On the other hand, the rotlet field (52) due to cell body rotation has a much more substantial influence on some other aspects of the flow analysed in Section 2. Above all, it limits significantly the values of R within which that flow's far field can take the simple vortical form depicted in Fig. 5. Because the main emphasis in this paper is on three-dimensional flow fields associated with helical movements, I now study this limitation in some detail.

The impossibility of any net torque acting on a self-propelling organism in Stokes flow, which leads in the case discussed here to the torque balance Eq. (46), excludes all possibility not only of a vortical far field of order R^{-1} like (29) but even of any rotlet far field of order r^{-2} like (52). Here, it is the flagellum's finite length – equal to L as measured along the centreline or $\ell = \alpha L$ along the x-axis – which already rules out any R^{-1} far-field behaviour for distances R comparable with ℓ, where it produces rather a transition to a rotlet field equal and opposite to (52) centred on the flagellum's mid-point. However, at such distances this is increasingly cancelled by (52) itself.

Details of the above process are shown in Fig. 9, plotting far-field velocities in the azimuthal direction (ϕ increasing) at three positions I,II and III (with, respectively, $x/\ell = 0.25$, 0.5 and 0.75) along the length of a flagellum, which acts on the field with a net torque $(-D\Omega, 0, 0)$ uniformly distributed along the distance $0 < x < \ell$ while a concentrated rotlet (52) of strength $(D\Omega, 0, 0)$ acts at the cell body position $x = 0$. The dotted line represents the vortical far field (29), while the two broken lines show only the effect of finite length of flagellum (i) at the midpoint II and (ii) at either of the quarter-length points III or I. These plots are computed, of course, as the azimuthal velocities associated with a uniform distribution of rotlets of strength $(-bh/\alpha, 0, 0)$ per unit axial distance x from 0 to ℓ, their total strength being $-bh\ell/\alpha = -bhL$. The solid lines add on the effect of the opposing rotlet of strength $bhL = D\Omega$ at $x = 0$; an effect which, as R/ℓ increases, becomes very marked – especially at the position I near the cell body. Moreover all the solid lines exhibit an absence of any significant far field at distances $R > \ell$.

The last two discussions yield opposite conclusions on the realism of the near-field and far-field features of the three-dimensional flow pattern around an unbounded helix analysed in Section 2. The near field (where the main viscous dissipation occurs) is negligibly influenced by superposition of the rotlet motions (52). On the other hand, analysis (Fig. 9) of the far-field behaviour shows that vortical far fields, typical (Fig. 5) of flows generated by an unbounded helix, become rapidly attenuated for increasing R (and vanish for $R > \ell$) in the case of a eukaryotic microorganism where a flagellum of finite length is attached at one end to the cell body. This conclusion, in its turn, can be contrasted with a later study (Section 5) of a highly specialised type of helical propulsion, characteristic of just a single bacterial order (Spirochaetales), which demonstrates how its three-dimensional flow field remains spatially

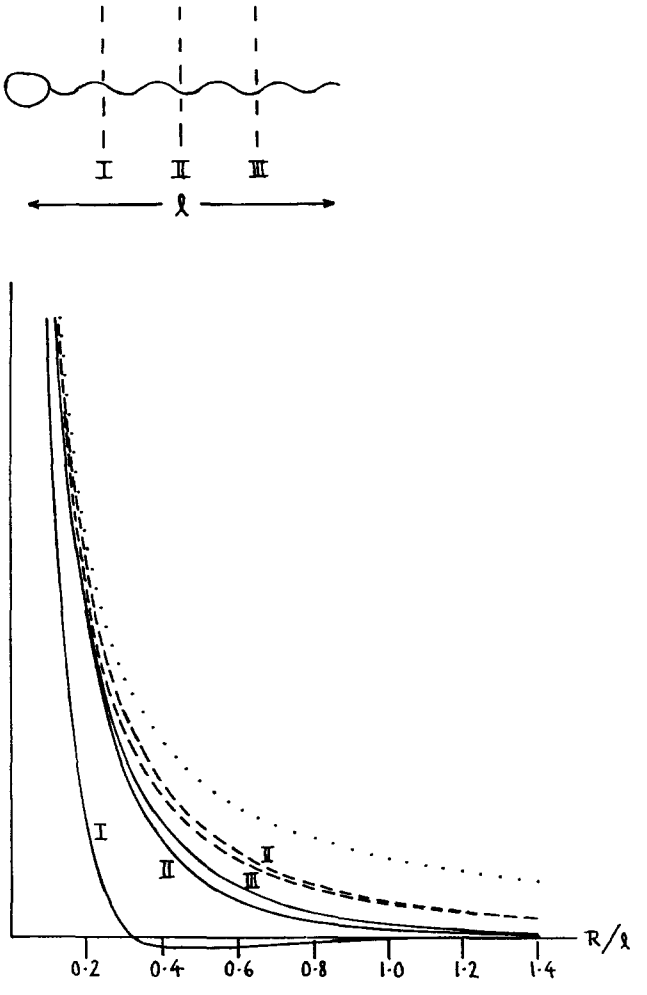

Fig. 9. For the case sketched (helical undulation of a single flagellum of axial extent ℓ, attached to a cell body that responds with a rotation resisted by an equal and opposite torque) the solid lines plot "far-field" values of azimuthal fluid motions in the planes I, II and III as functions of distance R from the axis. In each case the vortical far field calculated (Figs. 4 and 5) for an unbounded helix is given by the dotted line. The broken lines (the upper for plane II, and the lower for either III or I) show how this is modified just by the finite length of the flagellum, while the solid lines allow also for the opposing rotlet field associated with cell-body rotation.

concentrated – without any algebraically decaying terms in the far field – even when the helix is idealised as one of unbounded extent.

Now I return to the issue of how, in eukaryotic microorganisms, those inherent advantages for propulsive efficiency that are associated with helical undulation of a flagellum may be eroded by counterbalancing disadvantages related to cell-body rotation. In the simple single-flagellum case analysed so far, all disadvantages are encapsulated in the reduction factor (48), which diminishes the zero-thrust swimming speed U_0 generated by a given flagellar undulation while its reciprocal (see (51) above) augments the rate of working needed to produce a given swimming speed. The rest of Section 3 briefly interprets various features of microorganisms with two flagella in terms of the idea [1] that these may have evolved as methods for retaining the advantages of helical propulsion while its disadvantages were either (i) limited, (ii) annulled, or even (iii) transmuted into advantages.

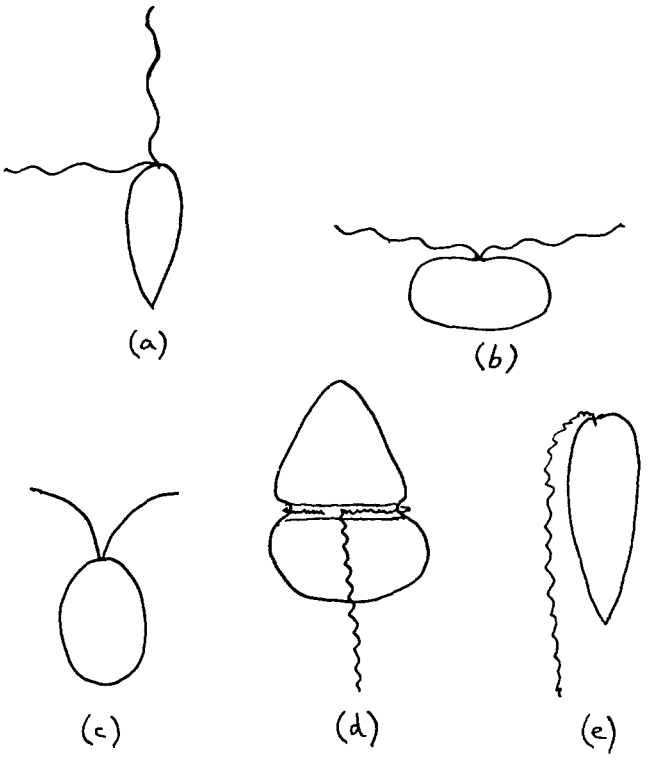

Fig. 10. Diagrammatically illustrating some eukaryotic microorganisms possessing two flagella: (a) *Procentrum* from the algal class Desmophyceae; (b) *Nephroselmis*, from the class Prasinophyceae; (c) *Chlamydomonas*, from the class Chlorophyceae; (d) a typical dinoflagellate *Gymnodinium*, showing its primary propulsive flagellum and a secondary transverse flagellum which beats in a groove let into the organism's external "armour"; (e) *Euglena*, showing the 180° bend near the base of its propulsive flagellum (by contrast, the secondary flagellum in *Euglena* is essentially vestigial).

First of all, it is clear that effects of the reduction factor (48) can be "(i) limited" by any substantial increase in D, the damping constant specified as resistive torque per unit angular velocity of cell body rotation. Such limitation seems to have been achieved in the algal class Desmophyceae. For example, the propulsive flagellum in the genus *Prorocentrum* (Fig. 10) pulls the organism forwards by means of a fast tip-to-base undulation (see [7], p.148) while a secondary flagellum – beating only slowly – stretches out a considerable distance at right angles to the swimming direction; such a big moment arm greatly increases that torque which resists cell rotation, so that D becomes much larger and effects of the reduction factor (48) are limited.

It is also clear, moreover, that the entire disadvantage associated with cell body rotation in response to the torque resulting from helical undulation of a flagellum can be "(ii) annulled" where an organism possesses two flagella able to execute equal helical undulations of opposite sense. Within the algal class Prasinophyceae, the genus *Nephroselmis* (Fig. 10) is commonly observed to move with both flagella undulating [8]. Here, the cell body does not rotate – just as would be expected if the undulations were both helical but exerted equal and opposite torques.

Again, among the green algae Chlorophyceae, the famous single-celled organism *Chlamydomonas* (Fig. 10), which commonly swims forwards by motions of its two flagella similar to

those of the human breaststroke, can be induced to beat a hasty retreat (escape reaction) with the flagella extended while undulations pass from base to tip along them. These would generate a high escape speed, and do so efficiently, if yet again they were equal helical undulations of opposite sense.

I note in passing that each of the three-dimensional flow fields associated with such a pair of opposed helical undulations includes a near field similar to that studied in Section 2. Their vortical far fields, on the other hand, tend to cancel out – which is yet another process acting to prevent the realisation of the far-field behaviour illustrated in Fig. 5.

Admittedly, controversy continues for certain organisms, including *Chlamydomonas*, about whether observed flagellar movements were broadly planar or broadly helical [9]. Indeed, because a three-dimensional undulation of a flagellum is seen under the microscope as its two-dimensional projection, helical undulations may have been reported as planar in some cases. Such helical undulations, on the other hand, can be presumed to have been present when rotation (or "gyration") of the cell body has been observed; indeed, some rotation may be expected even where two flagella execute opposite undulations, because the opposing torques are unlikely to be exactly equal. It is against this background that clear accounts of cell-body rotation in *Chlamydomonas*, both by Lowndes [10] (see pp. 119-120) and by Lewin [11] (who moreover reported it as being converted into a rapid spin when only one flagellum was beating) may perhaps be viewed as indicative of helical undulations.

I turn now to cases where disadvantages related to cell body rotation seem to have been "(iii) transmuted into advantages," arguing such an interpretation first for the dinoflagellates. As their name suggests, these are powerful single-celled organisms, amongst the larger of the flagellates, and are encased in formidable "armour". In addition to the propulsive flagellum which exhibits a base-to-tip undulation, dinoflagellates typically possess a "transverse flagellum", situated – and able to undulate – within a groove let into their armour (Fig. 10). Observations on *Ceratium tripos* showed [12] that the swimming organism usually displayed a substantial rotation about its direction of locomotion, but that the sense of this rotation was anticlockwise or clockwise according as the transverse flagellum (within its groove) was or was not beating.

Those observations strongly suggested [1] that the propulsive flagellum generates a helical undulation which, by itself, tends to produce a clockwise rotation of the body. On the other hand, the beating of the transverse flagellum in its groove is able to exert an anticlockwise torque that exceeds the clockwise torque associated with the helical undulation. Then the resulting sign change in the cell body's angular velocity Ω means that the effective angular velocity $\omega_E = \omega - \Omega$ can actually exceed ω.

This at once reverses one of the disadvantages linked with cell-body rotation, since Eq. (49) implies now not a reduction in the swimming speed U_0 but an enhancement (in fact, the corkscrew rotation now generated reinforces the ability of helical undulations to produce forward motion). Some more careful analysis may be required to identify the effects on rate of working for a given swimming speed, but an advantage can be glimpsed first of all in a case when the torque exerted by the transverse flagellum is just enough to cancel that exerted by the propulsive flagellum. In this case both the rotation Ω of the cell body and the energy dissipation $D\Omega^2$ associated with it must disappear from the total rate of working (50); being replaced merely with any rate of working by the transverse flagellum beating in its groove – expected to be less because of the limited volume of fluid set into circumferential motion. Next, as the torque applied by that flagellum is further augmented to make Ω negative, the swimming speed increases with a positive gradient while the extra dissipation rate $D\Omega^2$ increases at

first with zero gradient; suggesting that any overall optimum taking both considerations into account must be found for a negative value of Ω, as observed.

This section is now concluded with a description of microorganisms from the famous genus *Euglena* (Fig. 10). In *Euglena* the remarkable and superficially awkward arrangement of its one effective flagellum may have even more subtly turned what is potentially the main disadvantage of helical undulations into an advantage [1].

Viewed under a microscope *Euglena* displays quite clearly those cell body rotations which (as usual) result from the torque associated with the helical undulation of its flagellum (see pp.116–8 of [10], together with some valuable analysis in [13]). When it moves forwards, with this flagellum characteristically trailing from the anterior end (and giving thrust by a base-to-tip helical undulation) it seems inevitable that these rotations of the body must be transmitted past the 180° bend. (Indeed, all the indications are that axoneme structures are unable to sustain the high local torsion that would otherwise be required.)

It is, on the other hand, a familiar fact that a rotation in being transmitted by the torsional stiffness of a flexible filament around a 180° bend produces a complete reversal of the sense of its rotation in space. Moreover, if the resulting reversed rotation simply adds to the helical undulation a (reinforcing) corkscrew rotation with angular velocity $(-\Omega)$ instead of Ω, then the effective angular velocity ω_E becomes $\omega + \Omega$ instead of $\omega - \Omega$. When this substitution is applied in Eq. (48), the new value of (ω_E/ω) becomes

$$\frac{\omega_E}{\omega} = \left[1 - \chi \frac{4\pi\mu b^2 L}{D}\right]^{-1} . \tag{55}$$

Eq. (49) then implies a substantial enhancement of the swimming speed U_0.

This time, on the other hand, the increase in U_0 is not accompanied by any reduction in energy dissipation for a given swimming speed. A dissipation rate $D\Omega^2$ still accompanies cell body rotation, so that Eq. (50) continues to describe the total rate of working; moreover, its ratio to dissipation by flagellar movements alone takes (since ω_E is now $\omega + \Omega$) the value

$$\frac{\omega_E + \Omega}{\omega_E} = 2 - \frac{\omega}{\omega_E} = 1 + \chi \frac{4\pi\mu b^2 L}{D}; \tag{56}$$

exactly the same value as was implied by Eq. (51).

Nonetheless, the technique for swimming-speed enhancement used by *Euglena* is impressive. I note finally that it demands, in the region of the 180° bend, only a minimal amount of active sliding between adjacent tubules within the axoneme: just a revolving pattern of sliding at the frequency Ω of body rotation. This, of course, is a considerably less exacting requirement than the well established pattern revolving at frequency ω which I described at the beginning of Section 3.

4. Helical propulsion in bacteria

The bacteria are among those living cells which lack the spatially organised structures – incorporating membrane-bound nuclei and many other membrane-bound organelles – of eukaryotic cells. In each bacterium, rather, a single cytoplasmic membrane, inside the cell wall, bounds all the cell's fluid substance or cytoplasm. The mechanisms underlying their motility are also very different.

Actually, large numbers of bacterial species (including almost all the organisms of "coccus" shape – spherical or spheroidal) exhibit no active motility; while some other species –

with cells grouped, usually, into filamentous "trichomes" – are capable of various so-called "gliding" movements [1]. Nevertheless the vast majority of actively swimming bacterial cells derive their motility from the special properties of those bacterial flagella which, as I stressed in Section 1, are highly distinct in character from the flagella of eukaryotic microorganisms. They are thinner (of diameter 0.02 μm rather than the 0.2 μm shown in Fig. 1) and far more homogeneous. The protein, flagellin, of which each is composed (different, and yet only slightly different, in different bacterial species) has the capability, when in solution, of forming itself into flagella-like filaments, which take the form of helical tubes with empty central core. Commonly, a bacterial cell has many flagella, each being attached to it [1] by a short "hook" (with a similar, yet not identical, chemical composition) which enters through a hole in the cell wall into the region between that and the cytoplasmic membrane where a remarkable "rotary motor" is able to turn the flagellum.

I wrote my 1975 John von Neumann Lecture [1] when the existence of rotary motors driving bacterial flagella had only just been proved and I devoted ten pages (pp. 178-187) to an account of the overwhelming body of evidence for it which had by then been accumulated. Twenty years later these conclusions are well established [14] but readers interested in how that early body of evidence was pieced together may read about the details in those pages or elsewhere [15].

Here, rather, four different types of helical propulsion in bacteria are enumerated. Accounts of the first three types were sketched already in [1], but are now "filled out" with a little more detail as regards three-dimensional flow fields. The fourth type, however, on which is concentrated the last part of this section and the whole of Section 5, exhibits features which – although specially interesting from the biomechanics standpoint – were not described in [1]; and where the technique of Section 2 for studying the three-dimensional flow field proves particularly illuminating.

One of these four types of helical propulsion may be easiest to describe first even though it appears in rather few bacterial species; namely, those with just a single flagellum. They include *Pseudomonas citronellolis*, a somewhat isolated member of the huge genus *Pseudomonas* (within which the vast majority of species have several flagella). Taylor and Koshland showed [16] how its single flagellum, a left-handed helix, is driven by a rotary motor which normally turns it in the clockwise sense (looking along the flagellum from its base); so that the cell body with the flagellum trailing behind it is pushed forward by the thrust associated with such a corkscrew rotation. On the other hand, as in other bacteria (see below), the rotary motor occasionally goes into reverse for a period – during which the organism briefly retreats before making its next advance.

Again, the stalked bacterium *Caulobacter* (Fig. 11) pushes itself by the action of just a single flagellum at one end of the stalk during its motile phase, before ultimately using the stalk to attach itself to a substrate (see [17], p. 410). It is interesting to make comparisons between the pushing phase of the one and only flagellum in both these species of bacteria and propulsion by helical undulation as described in Sections 2 and 3.

Actually, as far as motions of the flagellar centreline are concerned, the similarities are very close indeed. Eq. (1) still represents its position at a general time t, and Eqs. (5) and (6) its movement at $t = 0$, provided that ω is here redefined as an angular velocity of corkscrew rotation relative to the cell body. Then c, similarly redefined as ω/k, becomes an apparent wave speed associated with that rotation (such as we observe, indeed, on turning a corkscrew). The only difference between the two cases lies in the fact that the entire cross-section of a bacterial flagellum rotates about the centreline (in contrast to the situation with eukaryotic

microorganisms), and this can be demonstrated experimentally (see [1], p.180); although (see later) it affects only negligibly the three-dimensional flow field.

Yet another similarity is that the corkscrew rotation at angular velocity $(-\omega, 0, 0)$ is opposed by a couple $(bh, 0, 0)$ per unit length which can act to determine the rotary movement of the entire organism at an angular velocity $(\Omega, 0, 0)$. Therefore, Eq. (7) still determines the effective angular velocity ω_E of the flagellar centreline relative to the ambient fluid; also Eq. (46), with D as the cell body's rotational damping constant, determines the value of Ω so that the ratio ω_E/ω is given by Eq. (48). Accordingly, the relationships between all quantities of direct biomechanical interest are once again exactly as shown in Fig. 1.

Next, as far as the three-dimensional flow field is concerned, it continues to take the form of a sum of the helical field calculated in Section 2 and the rotlet field (52) associated with cell body rotation at angular velocity Ω. However, both in *Caulobacter* and in *Pseudomonas citronellolis*, the origin of this rotlet field – taken at a central point within the body – tends to be somewhat farther removed from the flagellum itself than for the case illustrated in Fig. 9. This extends slightly, but only slightly, the distance beyond which it cancels out the equal and opposite rotlet far field due to the flagellum as a whole.

The strong similarity to helical propulsion in eukaryotic microorganisms, evident in the case of those exceptional bacterial species that are treated above, should not however lead us to expect such similarity for bacteria in general. In all those other types of helical propulsion in bacteria that are studied below, it has become significantly weakened.

Bacteria of the very next type are characterized as possessing substantial numbers of flagella, each of which takes the form of a left-handed helix. Moreover, when the associated rotary motors act normally to generate clockwise rotation, the various rotating helical flagella form into a bundle (or, occasionally, two bundles). Even though individual flagella cannot be resolved with a light microscope, the bundles can be seen (and seen very clearly [18] in oil-immersion dark-field microscopy) to assume also the form of left-handed helices. Furthermore, their corkscrew rotation is observed to push the bacterium forward on an approximately straight course.

On the other hand, an important difference from species with just one flagellum emerges during each of those brief periods when (simultaneously) all of the rotary motors go into reverse. The result is now by no means simply a retreat. Instead, the double event comprising an immediate flying apart of the different flagella in a bundle, quickly followed by a regrouping after the motors begin to turn clockwise again, seems to generate an almost completely random change in direction [19].

The mathematical theory of the "random walk" suggests how advantageously such random changes in direction might permit bacteria to achieve, on the average, a movement up the concentration gradient of any attractant molecule (or down the gradient for a repellent molecule) in a solution. Essentially, the bacterium needs to make variations in the frequency of those changes in direction; a frequency which should be kept low whenever the organism's chemoreceptors sense an increasing concentration of attractant (or decreasing concentration of repellent) while being raised to much larger values in the opposite situation. Berg and Brown comprehensively demonstrated [19] that this is exactly the behaviour displayed by bacteria of the type discussed here.

They form an enormous range of bacterial species. First, the majority of species in the previously mentioned "huge genus" *Pseudomonas* display several flagella, all emerging from two so-called "polar" regions; this is the case when the flagella may form two bundles. In

another genus *Selenomonas*, classified within the same order (Pseudomonadales), about 20 flagella all emerge [20] from a single polar region (Fig. 11).

In bacterial species belonging to the even bigger order Eubacteriales, flagella emerge from all round the organism – while tending nevertheless to form just a single bundle. Typical cases with six to eight flagella shown in Fig. 11 include *Proteus mirabilis* and *Bacillus megaterium* and are similar to the familiar *Escherichia coli* on which many of the experiments were done (an organism, *Salmonella typhosa*, with a far greater number of flagella is also shown).

The above second type of helical propulsion in bacteria, found so abundantly in nature, is actually the one concerning which the methods of this paper utilising helical distributions of stokeslets have rather little to tell us (other than "by analogy" and in very general terms). It would be hard to model the helical bundle convincingly by those means; in the present paper, therefore, this is the type which, even though commonest, has been discussed most briefly.

My last two types of helical propulsion in bacteria differ sharply from the first two, in that the organism's helical element is the cell body rather than any flagella. Also, the cell bodies concerned have considerably greater lengths (5 to 20 μm) than typical bacterial dimensions of 1 to 3 μm. Here, however, the list of common features between these last two types comes to an end.

Within the order Pseudomonadales, characterized by the existence (see above) of two polar regions (or occasionally just one) from which flagella emerge, members of the genus *Spirillum* display two such regions at the extreme ends of a helically shaped cell body (Fig. 11); however, the flagella are quite short compared with the cell body and are not helical to any significant extent. During motion, the flagella all rotate in the same sense about a longitudinal axis, exerting on the fluid a total torque T in that sense. The opposing couple T with which the fluid acts on the organism causes all of it, including the helical cell body, to rotate in the opposite sense, and it is this corkscrew rotation of the cell body itself which gives *Spirillum* its longitudinal motion (see [21] for a good biomechanical analysis and [22] for a still more accurate one using a Boundary Element method very close to the Lorentz approach; neither paper, however, being concerned with flow fields).

In *Spirillum volutans*, for example, the observed frequencies of complete revolutions (in opposite senses) take typical values 40 Hz for the flagella and 13 Hz for the cell body [23]; those values imply, of course, that the rotary motors are generating, relative to the cell body in which they are situated, revolutions at the compounded frequency of 53 Hz. For each flagellum it is the curved hook (see above) which is directly rotated, so that the flagella proper make an angle with the swimming direction and are perceived, when rotating, as "a blurred cone"; moreover, because the forward swimming movement (at a speed around 15 μm/s) applies drag forces to them, both cones of flagella are swept backwards to a certain extent (Fig. 12).

In relation to the themes of this paper, it may be interesting to observe that much of the analysis of Sections 2 and 3 continues to be applicable except that the part played there by the flagellum is here played by the helical cell body, while the complete ensemble of flagella fills the role there assigned to the cell body. With careful choice of notation to allow for this I use ω for the angular velocity (2π times the frequency in Hz cited above) at which the rotary motors turn the flagella relative to the cell body, and Ω for those flagella's observed angular velocity in space. Then the difference

$$\omega_E = \omega - \Omega \tag{57}$$

represents, of course, the cell body's angular velocity in the opposite sense – and the agreement between Eqs. (7) and (57) implies that much of the analysis of Section 2 can once again be

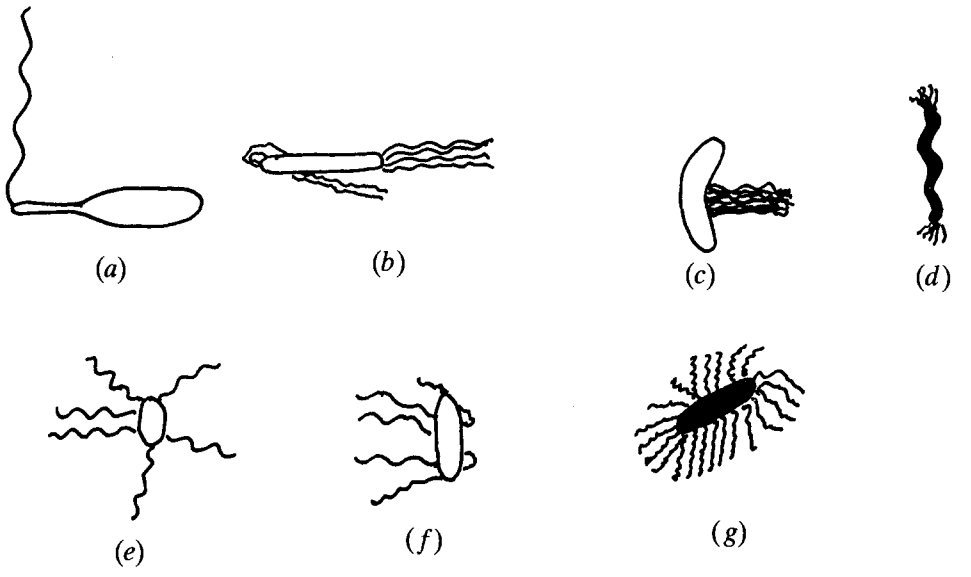

Fig. 11. Sketches of some bacteria that achieve motility by the action of rotary motors on thin, relatively passive flagella. (i) Bacteria from the order Pseudomonadales: (a) *Caulobacter*, with just a single flagellum; (b) a typical *Pseudomonas* species, with flagella emerging from two polar regions; (c) *Selenomonas*, displaying just a single polar region; (d) *Spirillum* (see also Fig. 12) with two polar regions from which there emerge flagella relatively short compared with the long helical cell body. (ii) Bacteria of peritrichous type (with flagella emerging all round the cell body) from the order Eubacteriales: (e) *Proteus mirabilis*, (f) *Bacillus megaterium*, (g) *Salmonella typhosa*.

used. Furthermore, if D is now defined as the rotational damping constant for the complete ensemble of flagella, rotating relative to the fluid at angular velocity Ω, then a balance between the torque $D\Omega$ resisting that rotation and the torque bhL in the opposite sense resisting the rotary movements of the cell body at effective angular velocity ω_E yields the same Eq. (46) as before with L as the cell body's length measured along the centreline. It is possible, therefore, to apply again all the results of Fig. 1 (where, however, the ratio $\Lambda/a = 25$ appropriate to the *Spirillum volutans* cell body needs to be used in place of greater values typical of eukaryotic flagella), alongside Eq. (48) for the ratio of the cell-body rotation speed ω_E to the angular velocity ω of the rotary motors.

As usual with the methods of this paper, the zero-thrust swimming speed U_0 derived in this way is slightly greater than the true swimming speed U – which is determined by the fact that the corkscrew rotation of the cell body needs to generate sufficient thrust to overcome the aforementioned drag experienced by the ensemble of flagella. Here, therefore, I should recall the explanation (Section 1) of the simple way in which the difference $U_0 - U$ is calculated, from a balance between the value of this drag at forward velocity U and the drag that would oppose the cell body's drift backwards, relative to the zero-thrust speed U_0, at velocity $U_0 - U$. (It is only in my last type of helical propulsion, soon to be described, that the zero-thrust and true swimming speeds become identical).

As regards the three-dimensional flow field around *Spirillum volutans*, its near field (close to the helical cell body) is expected to be much as shown in Figs. 3,4 and 5 (with allowance made for the reduced value of Λ/a); but, for reasons rehearsed already in Section 3, the far-field velocities must fall off at a vastly steeper rate. The cell body's finite length (L measured along the centreline, or $\ell = \alpha L$ measured along the axis of the helix) causes the vortical far

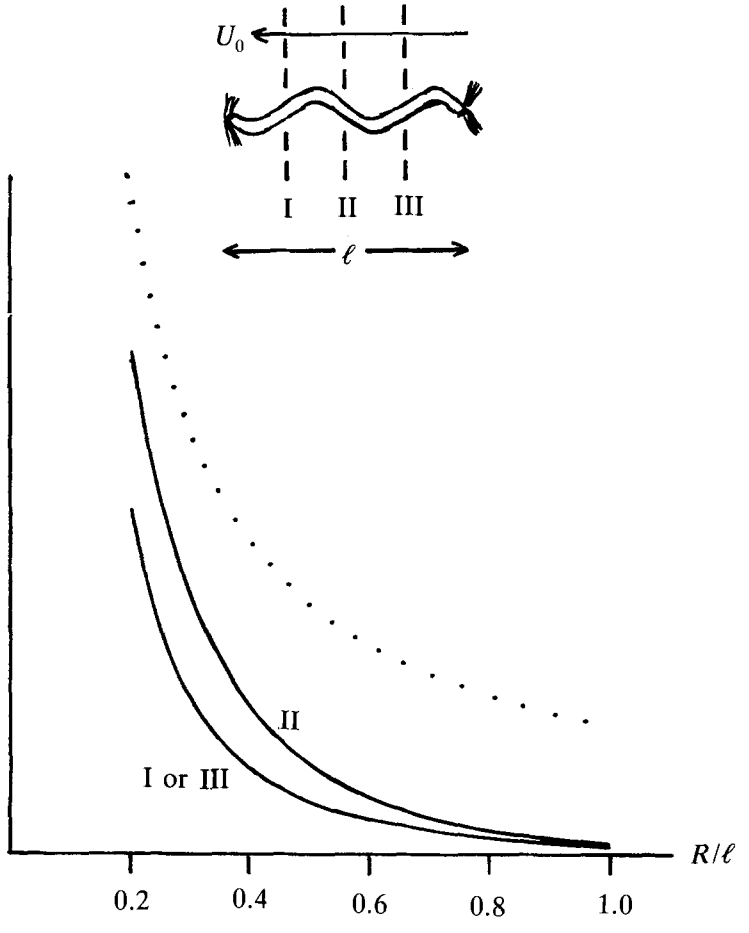

Fig. 12. In *Spirillum volutans* the flagella attached (by hooks) at each end of the cell body all rotate in the same sense, and the helical cell body responds with a rotation resisted by an equal and opposite torque. The latter rotation generates a swimming velocity – to the left in the case illustrated – which in turn gives both cones of rotating flagella a sweptback appearance. Also, "far-field" values of azimuthal fluid velocities are shown as function of distance R from the axis, with the dotted line giving the vortical far field calculated (Figs. 4 and 5) for an unbounded helix while the solid lines allow both for the finite length of the helical cell body and for two rotlet fields (associated with flagellar rotations at both ends).

field of Fig. 5 to be replaced by a rotlet far field of total strength bhL; however the rotlets of combined strength bhL in the opposite sense (representing the effects of flagella rotating at both ends of the body) produce once again a progressive cancelling of that far field which becomes complete for $R/\ell > 1$. (The only difference from the situation depicted in Fig. 9 is that the concentrated rotlet at $x = 0$ is replaced by half-strength rotlets at $x = 0$ and $x = \ell$. The effect of this, also shown in Fig. 12, is that the solid curve II remains unchanged, while both of the solid curves I and III are replaced by their arithmetic mean.)

Behaviour similar to that of *Spirillum* is found also in a few other genera. Recently, widespread attention was focussed upon *Helicobacter pylori*, whose presence in human stomachs has been convincingly linked [14] to pathological conditions including gastritis, peptic ulcer and stomach cancers. This too is a bacterium with a helical cell body and relatively short polar flagella.

Fig. 13. Dark-ground microphotograph (reproduced, with permission, from [14]) of some actively swimming spirochetes of the species *Treponema pallidum.*

I now conclude my analyses of helical propulsion with an account of the most remarkable type of all; where, although the helical external surface of the swimming organism can be observed to be performing corkscrew rotations which must generate torque, nevertheless there are no visible counter-rotations of flagella or other appendages to provide any opposing torque. These simple facts had been known for many decades during which however yawning gaps in communication between microbiological specialists making observations on bacteria and physical scientists familiar with angular momentum principles had limited the degree of wonderment elicited by the findings. With the vigorous growth of biomechanics in the 1960s, however, many scientists began to become aware of the enigma posed by established information on spirochete behaviour.

Spirochetes differ so much from other bacteria that they are classified as a separate order Spirochaetales, comprising just three genera *Treponema, Borrelia* and *Leptospira.* Fig. 13 shows the external appearance of *Treponema pallidum*, the agent of syphilis and yaws [14]; a similar exterior shape is common to other members of the order, including those responsible for half a dozen other serious diseases (*e.g.* Lyme disease). Every one of them swims by performing a corkscrew rotation about its longitudinal axis.

Much careful observation had been needed to establish beyond a doubt the absence of motile external appendages already referred to. Actually, outside the spirochete's external surface, there exist thin fibrils (usually three of them) but they do not move at all, being wrapped tightly around that surface in such a way that its helical shape is maintained (see [24], p.753). The point here is that a spirochete possesses a helical cell body outside which

there is a helical sheath, and the fibrils are required to maintain the good match in shape between the sheath and the cell body proper.

Just two flagella emerge, one from each end of the long helical cell body. However, they are situated entirely in the extremely narrow gap between that cell body and the external sheath. Accordingly, they are nowhere in contact with the ambient fluid – and so cannot be contributing any torque in opposition to that exerted on the ambient fluid by the organism's corkscrew rotation.

The enigma could be posed in either of two ways, both related to this torque with which the rotating organism acts on the fluid (which, conversely, acts on the organism with an equal and opposite torque):

(a) Steady rotation simply cannot be maintained against the opposing torque exerted by the fluid; moreover,

(b) because the organism's inertia is practically negligible, its rotation speed must be reduced to zero by viscous resistance in a time (related to cross-sectional radius squared divided by kinematic viscosity) of less than a microsecond.

Yet, even in the fact of these apparently insurmountable theoretical objections, the bacteria kept spinning along!

Only after the establishment (around 1974) of the existence of rotary motors driving bacterial flagella [15] did it first become possible to find a convincing biomechanical resolution of the enigma [25,26]; indeed this can in retrospect be perceived as having been the only possible resolution obeying fundamental angular-momentum principles. Here, that successful resolution is summarised before I go on to consider its implications for the external flow field.

The rotary motors cause each of the two flagella to turn in the same sense so that, at each cross-section (Fig. 14) within the above-mentioned narrow space between cell body and sheath, the flagella act as roller bearings that permit the sheath and the cell body to be in relative rotary motion. This is achieved by the sheath turning in one direction at rotation speed ω_S (the same all along the sheath) and the cell body turning in the opposite direction at rotation speed ω_B; where, if a_S is the internal radius of the sheath and a_B the external radius of the cell body, then $a_S\omega_S = a_B\omega_B$ (because both are equal to the circumferential velocity of the rotating flagella). To avoid misunderstanding I add that, although either of these rotation speeds (say ω_S) is uniform all along the cell body, nonetheless the corresponding angular velocity is a vector possessing uniform magnitude yet nonuniform direction – because its direction is always along the tangent to the sheath's centreline.

This rotation of each cross-section of the sheath about that sheath's local centreline is often called "self-rotation". It is, of course, opposed at each cross-section by a resistive torque due to fluid viscosity, and the resultant of all those torques on different cross-sections is a net torque about the axis of the helical organism. This, perforce, causes the organism to turn about that axis at an angular velocity ω_E, such that there is a precise balance between the net torque resisting self-rotation and the opposite torque resisting corkscrew rotation.

Clearly, the difficulties cited above as (a) and (b) now disappear, because the total torque acting between fluid and organism has become zero. Needless to say, there is viscous dissipation of energy in the fluid motion; however, such energy loss is restored by energy input from the rotary motors. (It may be interesting here to make a comparison with *Spirillum*, in which flagellar rotation produced by these motors yields directly the necessary torque between fluid and organism; by contrast, flagellar rotation in spirochetes is an intermediary in producing that self-rotation of the external sheath which now becomes responsible for torque generation.)

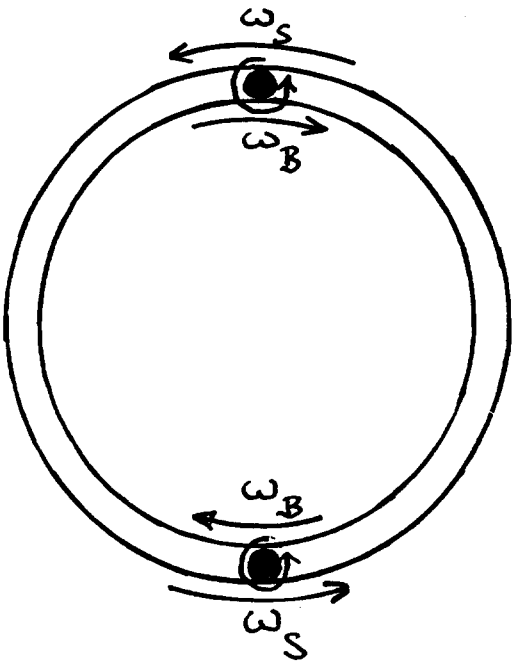

Fig. 14. Sketch, following Berg [26], of the cross-section of a spirochete's helical cell body and of its closely fitting external sheath, showing the "roller bearing" action of the rotating flagella between the sheath's inner surface and the cell body's outer surface. These rotate in opposite directions with rotation speeds ω_S and ω_B respectively.

Because Stokes flows satisfy linear equations, the three-dimensional flow field associated with the combined self-rotation and corkscrew rotation of spirochetes is a linear combination of the flow field that would be associated with each separately. For corkscrew rotation at angular velocity ω_E, an unbounded-helix model of the associated flow field has been comprehensively analysed in Section 2. Before deriving the corresponding self-rotation model, I emphasize that the present problem is one where the whole is greater in value than the sum of its parts. This is because the two fields have equal and opposite axial torques per unit length; accordingly, their vortical far fields cancel and we shall see that the combined flow field is highly localised. This makes an unbounded-helix model rather specially appropriate for studying the three-dimensional flow field in the neighbourhood of a swimming spirochete.

In order to model the flow field due to self-rotation, distributed rotlet fields are clearly needed. Eq. (52) described a concentrated rotlet field generated when a torque $(D\Omega, 0, 0)$ in the x-direction is applied at the origin; evidently, its numerator is the vector product of that torque and the displacement (x, y, z) from its point of application. It follows that a flow which takes the form of distributed rotlet fields of strength $\mathbf{J}(s)$ per unit length along the helix (4) can be written in terms of the vector product $\mathbf{J}(s) \times \mathbf{r}_0$ as

$$\int_{-\infty}^{\infty} \frac{\mathbf{J}(s) \times \mathbf{r}_0}{8\pi\mu r_0^3} \mathrm{d}s; \tag{58}$$

where, as in Section 2, the vector $\mathbf{r}_0$ represents displacement of a field point from the location (4) of the singularity. Here $\mathbf{J}(s)$, the torque exerted per unit length by self-rotation, is expected to be of uniform magnitude while at each point its direction is along the tangent to the helical centreline.

Amusingly, this vector $\mathbf{J}(s)$ has properties (uniform magnitude and tangential direction) identical with those of a steady current in a wire, and the famous law of Biot and Savart tells us that expression (58) is proportional to that current's magnetic field. Yet, even though the magnetic field due to a current in a helical coil of wire has undoubtedly been computed many times, I found it convenient in pursuing my objective of superimposing results on those of Section 2 to compute directly the flow field (58).

A specially striking feature of the Biot-Savart law is its declaration that the vector field (58) is necessarily irrotational. Thus, even though the flow field (52) of an individual rotlet, corresponding to the far field of a rotating body, has nonzero vorticity, nonetheless all vorticity cancels out in the distribution (58) of rotlet fields.

In purely hydrodynamic terms (without bringing in electromagnetic doctrines) expression (58) can be recognized as the irrotational flow field induced by a (curved) line vortex of strength

$$\frac{J}{2\mu}, \tag{59}$$

where J is the uniform magnitude of the tangential vector $\mathbf{J}(s)$; see also [27] for further analysis of this case. Of course, the real fluid flow does not extend to the singular location of the line vortex itself (the sheath's centreline) but just to a distance a from it, where a is the sheath's external radius. At that distance, the fluid rotates about a vortex of strength (59) with rotation speed

$$\omega_S = \frac{J}{4\pi\mu a^2}, \tag{60}$$

which must evidently coincide with that of the sheath's external surface. (Although it is well known that a straight circular cylinder which rotates so as to exert a torque J on the fluid creates outside itself a vortical motion of strength (59), and also that viscous stresses in this irrotational flow transmit the same torque outwards across every distance R from the axis of the cylinder, nonetheless it appears quite interesting that an external irrotational motion can be generated even in the case of a self-rotating helical shape.)

Now, in order to model flows around swimming spirochetes, it is necessary to combine the flow (12), generated by a corkscrew rotation (at angular velocity ω_E) that exerts on the fluid a net torque $(-bh)$ about the x-axis, with a flow (58) due to self-rotation for which the net torque about the x-axis takes an equal and opposite value $(+bh)$. Then the vector $\mathbf{J}(s)$ is a multiple (bh/α) of the unit tangent vector to the helix (4), giving

$$\mathbf{J}(s) = \frac{bh}{\alpha}(\alpha,\ -bk\sin ks,\ bk\cos ks). \tag{61}$$

Moreover the expression (58) for the self-rotation field, with Eq. (15) for the displacement $\mathbf{r}_0$ of a field point from the helix, becomes

$$\begin{aligned}\frac{8\pi\mu\mathbf{u}}{h} = \frac{b}{\alpha}\int_{-\infty}^{\infty} [&-Rbk\cos(ks-\phi) + b^2k\ ,\\ &-R\alpha\sin\phi + \alpha b(\sin ks - ks\cos ks),\ R\alpha\cos\phi - \alpha b(\cos ks + ks\sin ks)]\ \tfrac{ds}{r_0^3};\end{aligned} \tag{62}$$

which, after the substitutions (20) used for purposes of nondimensionalisation, takes the form

$$\frac{\beta}{\alpha}\int_{-\infty}^{\infty}\frac{[\beta^2(1-X\cos(\theta-\phi)),\ \alpha\beta(\sin\theta-\theta\cos\theta-X\sin\phi),\ \alpha\beta(X\cos\phi-\cos\theta-\theta\sin\theta)]}{[\alpha^2\theta^2+\beta^2(X^2-2X\cos(\theta-\phi)+1)]^{3/2}}\mathrm{d}\theta. \tag{63}$$

Next, because of the need (as in Section 2) to apply the basic theorem of flagellar hydrodynamics [5], I focus first on field points with $\phi = 0$ which include the location $X = 1$, $\phi = 0$ of the helix itself. Here, because once again the integrand's denominator becomes an even function of θ, expression (63) can be simplified by combining values of the integrand for θ and $-\theta$ to give

$$\frac{4\pi\mu\mathbf{u}}{h} = \left[\frac{\beta^3}{\alpha}\left(\tfrac{1}{2}XB_3 - B_4\right),\ 0,\ \beta^2(B_4 + \tfrac{1}{2}B_3 - B_1)\right], \tag{64}$$

where $B_1(\alpha, X)$ is defined in Eq. (22) and where

$$\{B_3(\alpha,X),\ B_4(\alpha,X)\} = \int_0^{\infty}\frac{\{2(1-\cos\theta),\ X-1\}}{[\alpha^2\theta^2+\beta^2(X^2-2X\cos\theta+1)]^{3/2}}\mathrm{d}\theta. \tag{65}$$

Now a simple asymptotic estimation shows that the pure vortical motion about the centreline is represented entirely by the B_4 integral, which has the limiting property

$$B_4(\alpha,X) - \frac{1}{\beta^2(X-1)} \to -\tfrac{1}{2} \quad \text{as } X \to 1. \tag{66}$$

Thus the other terms in (64) represent distortions of the local motion associated with the curved shape of the line vortex.

Out of these, it was shown in Section 2 that $B_1(\alpha, X)$ becomes logarithmically infinite as $X \to 1$, but that the basic theorem of flagellar hydrodynamics relates the actual motion of the flagellar cross-section to a function $A_1(\alpha)$ which Eq. (23) defines in terms of the integral for $B_1(\alpha, 1)$ over a range with the small interval $0 < \theta < \epsilon$ excluded. Now a function $A_3(\alpha)$, plotted in Fig. 15, may be similarly defined so that

$$-\ln\epsilon + A_3(\alpha) = \int_{\epsilon}^{\infty}\frac{2(1-\cos\theta)}{[\alpha^2\theta^2+2\beta^2(1-\cos\theta)]^{3/2}}\mathrm{d}\theta, \tag{67}$$

where once again the integrand is asymptotic to θ^{-1} as $\theta \to 0$.

The existing form of the basic theorem of flagellar hydrodynamics [5] describes the motion of a local cross-section associated with a distribution of stokeslets along the centreline. The corresponding result for a distribution of rotlets is extremely similar (see Appendix) although it involves the addition of an extra term $\frac{1}{2}$ (rather than either 1 or 0) wherever $\ln\epsilon$ occurs; and, of course, it just describes elements of the local motion other than the cross-section's simple self-rotation about the centreline.

Application of this result leads to equations, supplementary to Eqs. (26), for the helical-vortex contributions to the zero-thrust swimming velocity U_0 and the angular velocity ω_E of corkscrew rotation. They are obtained from Eq. (64) by omitting the self-rotation terms so that B_4, by Eq. (66), is replaced by $-\frac{1}{2}$. Then the cross-sectional velocity (8) for $s = 0$ is equated

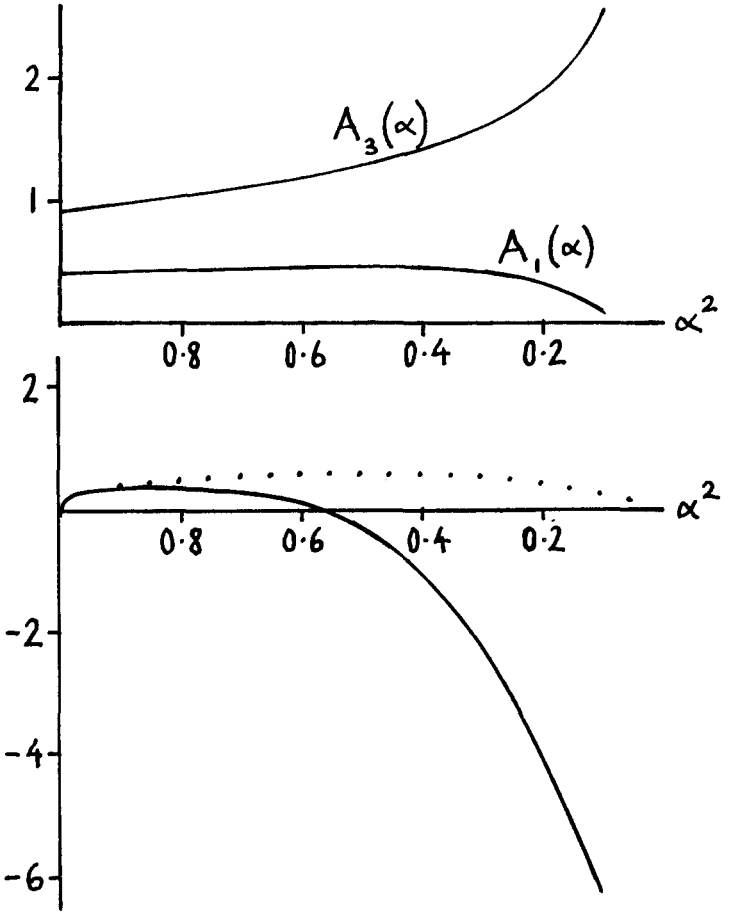

Fig. 15. If a helical shape executes self-rotation, necessarily found alongside a corkscrew rotation resisted by an equal and opposite torque, their effects on the swimming velocity U_0 are governed by Eqs. (68) and (26) with $A_3(\alpha)$ and $A_1(\alpha)$ taking values plotted as functions of the axial direction cosine α in the upper diagram. These effects on U_0 are of opposite sign: in the lower diagram the dotted curve shows the positive value of $4\pi\mu U_0/h$ given by (26) alone, while the solid line shows the combined value with the negative effect (68) of self-rotation added on. Although corkscrew rotation dominates for large α, its influence on swimming velocity becomes almost negligible for values of α^2 around 0.1 as found (Fig. 13) in *Treponema pallidum*. (In computing these curves, a value $\Lambda/a = 32$ was used, corresponding to $a = 0.1\mu$m and to $\lambda = \alpha\Lambda = 1\mu$m as in *Treponema pallidum*.)

to the results of putting $X = 1$ in the other terms, with a substitution of $(-\ln\epsilon + A_3(\alpha) - \frac{1}{2})$ for B_3 and of $(-\ln\epsilon + A_1(\alpha) - \frac{1}{2})$ for B_1. This leads to expressions

$$\left.\begin{aligned} 4\pi\mu U_0/h &= -\tfrac{\beta^3}{2\alpha}\left(-\ln\epsilon + A_3(\alpha) + \tfrac{1}{2}\right), \\ 4\pi\mu\omega_E b/h &= \beta^2\left[-\ln\epsilon + A_1(\alpha) - \tfrac{1}{2}(-\ln\epsilon + A_3(\alpha) - \tfrac{1}{2})\right] \end{aligned}\right\} \tag{68}$$

for those contributions, additional to Eqs. (26), which are induced by the helical vortex.

The results of adding Eqs. (26) and Eqs. (68) affect quite differently the swimming velocity U_0 and the angular velocity ω_E of corkscrew rotation. The latter is changed only moderately by the new contribution (68). By contrast, the corresponding contribution (68) to the swimming velocity U_0 is of an opposite (negative) sign, and also has the possibility of being much larger in magnitude, particularly for relatively small α.

Fig. 15 shows as a function of α^2 the competing effects of self-rotation and of corkscrew rotation under conditions of zero net torque about the x-axis. These, of course, are the conditions which determine the self-rotation torque vector as in Eq. (61), including a factor α^{-1} in its y- and z-components; which, in turn, are the components that contribute to the x-component of cross-section velocity. Here is one reason why the self-rotation effects dominate the swimming velocity for small α.

Yet another, more hydrodynamically fundamental reason is associated with the capacity of a helical line vortex to induce motions of itself parallel to its axis. Once again, it is particularly as α becomes smaller (when the helical vortex begins to share properties with a chain of vortex rings) that this self-induced motion is intensified – a trend which, mathematically, is expressed by $A_3(\alpha)$ becoming quite large for small α (Fig. 15).

Actually, Fig. 15 shows how corkscrew rotation effects are paramount for larger α^2 and self-rotation effects for small α^2. Around $\alpha^2 = 0.5$ (the condition (27) that gives greatest efficiency to the swimming of eukaryotic microorganisms by helical undulation of flagella), the two effects cancel and it would hardly be possible for a spirochete to swim at all! Larger values of α^2 might produce a form of swimming dominated by the action of corkscrew rotation. On the other hand, a spirochete must gain very substantial benefits from self-induced motion effects if, as observed, α^2 is relatively small. In that condition corkscrew rotation is still present; however, the direction of swimming is the opposite of that expected from the action of such rotation by itself (in other words, swimming direction has contrary relationships to sense of corkscrew rotation in *Spirillum* and in spirochetes). Against this background it is interesting to note that the case $\alpha^2 = 0.1$, $\beta^2 = 0.9$ corresponds to the ratio λ/b of pitch to radius for the helix taking a value

$$\frac{\lambda}{b} = \frac{\alpha\Lambda}{b} = \alpha\frac{2\pi}{bk} = 2\pi\frac{\alpha}{\beta} = \frac{2\pi}{3} = 2.1, \tag{69}$$

which is close to that observed in microphotographs of swimming spirochetes such as Fig. 13.

It is valuable next to probe the relationships between the swimming velocity U_0 and the angular velocity ω_S of self-rotation of the sheath. (Here, the adjectival phrase "zero-thrust" can be omitted in describing this swimming velocity U_0 because the helical shape comprises the entire organism so that there exists no possibility of an additional part of the organism being subjected to any drag which would need to be overcome by the helix exerting any thrust.) Now, by Eqs. (60) and (61),

$$\omega_S = \frac{bh}{4\pi\mu a^2\alpha}, \tag{70}$$

and it follows from the first of Eqs. (68) that the swimming velocity U_0 directly induced by self-rotation is in a ratio to the latter's circumferential velocity equal to

$$\frac{U_0}{a\omega_S} = -\frac{a}{b}\left[\frac{\beta^3}{2}\left(-\ln\epsilon + A_3(\alpha) + \tfrac{1}{2}\right)\right]. \tag{71}$$

Numerically, this is greatest for a given ratio a/b of sheath radius to helix radius when the quantity in square brackets is greatest, which (see Fig. 15) requires α^2 to be small. Moreover, these are conditions when U_0 is rather little affected by the countervailing effect of corkscrew rotation.

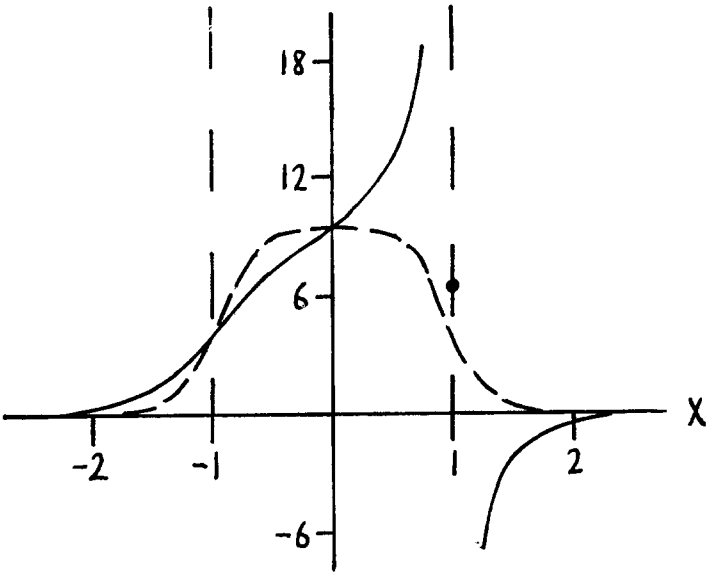

Fig. 16. Illustrating axial fluid motions (x-components of $4\pi\mu u/h$) computed with $\alpha^2 = 0.1$ for the flow around a swimming spirochete in the plane $x = 0$ intersected by the helical centreline at the point $y = b$, $z = 0$. As in Fig. 3, the solid line gives values on the y-axis with $X = y/b$ while the broken line gives values on the z-axis with $X = z/b$. Axial velocities between the two vertical broken lines are all positive, corresponding to a large positive flux through the coils of a swimming spirochete at a mean velocity exceeding the spirochete's own velocity (represented by the blob).

5. Flow field around a swimming spirochete

After the above synopsis of that basic biomechanics of spirochete locomotion which was first developed two decades ago [25], I proceed finally to a description of the associated three-dimensional flow field. This could be expected to be highly localised as a result of the cancellation of far fields associated with equal and opposite axial torques due to self-rotation and to corkscrew rotation; yet the sharp localisation actually found (with essentially, no penetration of the flow beyond a distance of twice the helix radius from its axis) is quite surprising, while indicating too that flow fields around real spirochetes of finite length may be rather well represented by the present model using an unbounded helix. The computations have been carried out for the value $\alpha^2 = 0.1$ suggested by the above discussion – a value in sharp contrast to the case (27) used in Section 2 for the analysis of flow fields around flagella of eukaryotic microorganisms. As before, the three-dimensional flow field is computed on the plane $x = 0$; the flow field on any other plane $x =$ constant being obtained from this by a simple rotary displacement.

Fluid velocity components in the x-direction (parallel to the axis of the helix) are shown in Fig. 16. Here, just as in Fig. 3, the solid line gives the x-component of $4\pi\mu u/h$ on that axis $z = 0$ which passes through the location $(0, b, 0)$ of the helix itself; this is the sum of contributions (for $\phi = 0, \pi$) from the x-components of (21) and (64). The broken line, again as in Fig. 3, shows how the same quantity varies on the perpendicular axis $y = 0$; here, it is derived from the x-components of (19) and (63) for $\phi = \pm\pi/2$. Both distributions become negligible (as mentioned above) when $|X| = R/b > 2$.

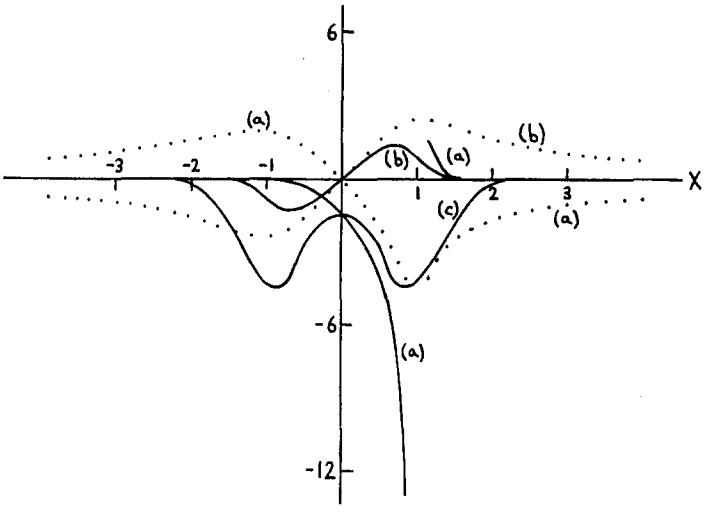

Fig. 17. Illustrating fluid motions at right angles to the axis of the helix for a swimming spirochete. As in Fig. 4, the solid lines give computed components of $4\pi\mu\mathbf{u}/h$ as follows: (a) its z-component on the y-axis (where however the y-component vanishes) with $X = y/b$, alongside (b) its y-component and (c) its z-component on the z-axis, both with $X = z/b$. All these "in-plane" velocity components in Fig. 17 share with the axial components in Fig. 16 the property that they become negligible for $|\ X\ | > 2$; that is, at distances from the axis exceeding twice the radius of the helix. In the case of curves (a) and (b) this property is in sharp contrast to the behaviour (given by the dotted lines, with their vortical far fields) associated with the effects of corkscrew rotation alone. When the opposing effects of self-rotation are added on (solid lines), such vortical far fields disappear.

Actually, the distribution of axial velocity (unlike that of azimuthal velocity studied below) is in both cases found to be dominated by the self-rotation contributions (64) and (63); just as the swimming velocity U_0 was found earlier to be dominated for $\alpha^2 = 0.1$ by the self-rotation contribution (68). In Fig. 16, a blob at the location $X = 1$ of the helix itself indicates the organism's own axial velocity (where the negative value of U_0 corresponds by (8) to a positive value for the x-components of $\mathbf{u}$), and the solid line exhibits a vortical behaviour close to the helix centred upon this blob.

Perhaps the most striking feature of Fig. 16 is that both curves display a large positive flow in the cylindrical region $y^2 + z^2 < b^2$ interior to the helix (the region between the two vertical broken lines); it corresponds in the electromagnetic problem, of course, to the strong axial magnetic flux induced inside a coil of wire along which a current passes. This powerful interior flow through the coils of a swimming spirochete (at an average velocity exceeding that of the organism itself) may be a specially important conclusion of this paper. (Evidently, it is in sharp contrast with the absence of any mean axial flow for the case illustrated in Fig. 3.) But before commenting further on this conclusion I outline computational results for velocity components in a plane perpendicular to the axis of the helix.

The solid lines (a), (b) and (c) in Fig. 17 (where, actually, the vertical scale is expanded twofold compared with that in Fig. 16) have meanings exactly as specified in Fig. 4. However, in sharp contrast to Fig. 4, these distributions again exhibit rapidly decaying far fields, essentially negligible for $|X| > 2$.

For example, curve (a) plots the z-component of $4\pi\mu\mathbf{u}/h$ on the axis $z = 0$, while curve (b) plots its y-component on the axis $y = 0$; both, then, are distributions of azimuthal components of velocity. Yet both distributions have become highly localised, even though the

corresponding curves in Fig. 4 possess vortical far fields (as shown, too, by a replot of the same data in Fig. 5).

In the case of these azimuthal components of velocity, a rather even balance exists between the contributions of corkscrew rotation (associated with a distribution of azimuthally directed stokeslets) and self-rotation (represented by rotlets). Indeed, dotted lines in Fig. 17 show the form of curves (a) and (b) associated with just a corkscrew rotation by itself. They are similar in character (though not identical, because computed for $\alpha^2 = 0.1$ rather than $\alpha^2 = 0.5$) to the analogous curves (a) and (b) in Fig. 4; and, in particular, they have substantial vortical far fields. It is only because the corresponding curves (a) and (b) due to self-rotation (generating equal and opposite axial torque) have equal and opposite far fields that the solid-line curves (a) and (b), representing the sum of both effects, lack any such far fields. (Incidentally, it may be noted that the solid line (a) exhibits near the helix $X = 1$ a vortical behaviour due to self rotation, centred upon a negative azimuthal motion associated with corkscrew rotation).

Only curve (c), which shows how the z-component of $4\pi\mu\mathbf{u}/h$ is distributed on the axis $y = 0$, was found already in Fig. 4 to be highly localised. That distribution has in Fig. 17 become even more localised; on the other hand, the computed contribution from corkscrew rotation to this curve (c) in Fig. 17 turns out to be relatively insignificant. In other words, curve (c) as shown is very close to the distribution associated with self-rotation alone, and it may be interesting to ask why this generates a substantial z-velocity on the axis $y = 0$.

To answer this question it is necessary to recall that velocity distributions in any plane x=constant are obtained from those in the plane $x = 0$ by a simple rotary displacement through an angle kx/α. (Eq. (1) for the helix itself shows first how s becomes x/α, and then how the angle ϕ defined in Eq. (14) increases by kx/α.) It follows that x-derivatives of velocity components are $(-k/\alpha)$ times ϕ-derivatives (axial and azimuthal gradients are in this constant ratio). Such considerations allow the characteristics of curve (c) for the z-component of $4\pi\mu\mathbf{u}/h$ on $y = 0$ to be viewed primarily as consequences of the equation of continuity, relating the z-derivative of this z-component to minus the x-derivative of the x-component, and so to $(+k/\alpha)$ times its ϕ-derivative. Broadly, this suggests that the right-hand half of curve (c), giving results for $\phi = \pi/2$, should have positive or negative gradient according as the x-components of $4\pi\mu\mathbf{u}/h$ shown in Fig. 16 exhibit and increase or decrease from $\phi = 0$ to $\phi = \pi/2$, and this broad expectation is borne out in practice.

For all the curves in Figs. 16 and 17, the steep rate of decline as x increases is associated with the axial wavenumber k/α which has just been identified. Indeed, for this axial wavenumber, solutions of the Stokes equations without vortical far fields have asymptotic behaviours which include (alongside algebraic factors) an exponential factor

$$e^{(-k/\alpha)R} = e^{(-\beta/\alpha)X} \text{ (because } R = bX \text{ and } \beta = bk). \tag{72}$$

For $\alpha^2 = 0.1$ this is e^{-3X} whereas for $\alpha^2 = 0.5$ it is e^{-X}; a contrast which explains both the still greater localisation for curve (c) shown in Fig. 17 as against Fig. 4, and that found in the curves of Fig. 16 by comparison with those of Fig. 3.

Nonetheless the most important feature of Fig. 16 (and one which also is in complete contrast to Fig. 3) is the large positive flux through the coils of a swimming spirochete. This strong interior jet-like flow (at an average velocity exceeding that of the organism itself) is potentially advantageous for the life-style of these bacteria. Thus, as a spirochete moves forwards, it is continuously exposed around the outside of the helix to new fluid approaching from in front, while at the same time a jet of fluid coming from behind passes through the interior of the helix. Both features should combine to bring a rather rapid flow of nutrients (as

well as of chemical signals) towards the spirochete's close proximity and so help to maintain its energetic swimming movements.

6. Conclusions

Helical distributions of stokeslets offer a useful approach towards modelling four types of zero-thrust swimming:

(i) that associated with single-celled eukaryotic organisms (algae and protozoa) which utilise active sliding movements of internal tubules within the axoneme to generate helical undulations of a propulsive flagellum;

(ii) that associated with the action of a rotary motor at the base of a thin corkscrew-like passive flagellum of a bacterium;

(iii) that associated with a bacterial cell body of helical shape, which acquires a corkscrew rotation when bunches of relatively short flagella at both ends are set into rotary movement by such motors; and

(iv) that associated with spirochete swimming, where just two flagella are caused by rotary motors to act as roller bearings between a helical cell body and an external sheath which they excite into self-rotation about its own (helically curved) axis.

Only in case (iv) is the zero-thrust swimming speed U_0 the same as the actual speed. In other cases U_0 is a little greater than the organism's true swimming speed U, which is modified by the need for helical movements to generate enough thrust to overcome the drag of *either* the cell body in cases (i) and (ii) *or* the spinning flagella in case (iii). The difference $U_0 - U$ is determined in such cases from a balance [1] between this drag, at speed U, and a thrust which essentially consists of hydrodynamic resistance to the helix's backward drift at velocity $U_0 - U$ relative to the zero-thrust motion.

Helical undulation (see (i) above) minimises, for given U_0, the flagellum's rate of working all along its length if $\alpha^2 = 0.5$ (where α is the helix's axial direction cosine); but this advantage may be diminished by effects of the hydrodynamic torque which ipposes that undulation. By causing the whole organism to rotate at angular velocity Ω, it reduces the effective rotation speed of the helix from ω (the undulation's radian frequency) to a value $\omega_E = \omega - \Omega$, determined by a balance between torques opposing the cell body's and flagellum's rotation at speeds Ω and ω_E. This reduction, producing a similar fall in U_0, may however be eliminated where two flagella execute helical undulations in opposite senses. Moreover, it may be changed into actual increases in ω_E and U_0 in two groups of microorganisms: dinoflagellates, where a secondary flagellum beating in a groove exerts active torque in an opposite sense; and euglenids, where the cell body's rotation, transmitted around a 180° bend at the flagellum's base, gives the undulation an effective rotation speed $\omega_E = \omega + \Omega$.

To a survey of these features previously described [1], the present paper adds an analysis of the flow field of that helical distribution of stokeslets which models zero-thrust swimming. In any plane perpendicular to the axis of the helix, motions parallel to that axis are found to have zero means; indeed, their azimuthal average is zero at each distance from the axis. In particular, fluid motion at speed U_0 near the organism's surface is reciprocated by neighbouring equal and opposite motions of fluid (Fig. 3), a conclusion interpreted in Fig. 6 from the geometrical nature of stokeslet fields. Yet motions in the plane itself are far less localised, being dominated (Fig. 5) by the vortical far field associated with the axial torque acting on the fluid. Nevertheless, where this torque is counteracted by an equal and opposite torque due to cell-body rotation, with its

far field described by the rotlet singularity (curl of a stokeslet), the flow field of the organism as a whole falls off much more rapidly (Fig. 9).

Fluid motions in case (ii) are extremely similar for those relatively few bacterial species that possess just a single helical flagellum, to which a rotary motor impacts an angular velocity ω relative to the cell body. This, as before, is given a rotation speed Ω in the opposite sense by the torque that resists flagellar movement. On the other hand, the far commoner case of a bacterium propelled by a bundle of rotating helical flagella is not well suited to accurate modelling by helical distributions of stokeslets.

In case (iii), typified by *Spirillum*, such modelling comes back into its own. Using ω again for the angular velocity of all of the flagella (in the same sense) relative to the cell body, but this time expressing their observed angular velocity in space as Ω, we recognize the difference $\omega_E = \omega - \Omega$ as the rotation speed of the cell body. This corkscrew rotation generates the zero-thrust swimming speed U_0 while the relation of ω_E to ω is determined by a balance between the torques opposing the rotations of the cell body and the flagella at speeds ω_E and Ω. Then the helical distribution of stokeslets has the same flow field as before, except that aximuthal motions in the far field are modified this time by the fields of two rotlets, one at each end of the helix (Fig. 12).

Finally, for spirochetes (see (iv) above), the "self-rotation" of the helical sheath, with each cross-section rotating about its own axis, can be modelled by a distribution of tangentially directed rotlets along that helically curved axis. The net axial torque which resists these movements causes the whole organism to undergo a rigid corkscrew rotation – represented in turn by a helical distribution of azimuthally directed stokeslets – in such a way that no net axial torque acts between the organism and the fluid. For such a combination the swimming velocity U_0 incorporates oppositely directed contributions from self-rotation and corkscrew rotation (Fig. 15), but large swimming velocities emerge for small values of α^2, around the value $\alpha^2 = 0.1$ observed (Fig. 13) for *Treponema pallidum*, when the self-rotation effect dominates all axial motions including the swimming velocity.

By contrast, self-rotation and corkscrew rotation produce comparable effects on azimuthal motions, so that their vortical far fields cancel (Fig. 17). Indeed, analysis for $\alpha^2 = 0.1$ shows the whole fluid motion around a spirochete to be confined to distances from the axis of less than twice the radius of the helix. This suggests that flow fields calculated for a distribution of such rotlets and stokeslets along an unbounded helix may model rather accurately the motion near a real spirochete of finite length.

The most important conclusion from this model is that axial motions (Fig. 16), far from poseessing any zero mean across a plane perpendicular to the axis, are instead dominated by a powerful interior flow (at an average velocity exceeding U_0) through the coils of the spirochete. Such jet-like interior motions are expected to be advantageous for the life-style of these bacteria.

In this long paper, a unified approach to the study of many features of the hydrodynamics of microorganism locomotion has been fruitfully applied. The approach adopted, moreover, has been directly derived [5] from the great discoveries made in 1896 by H. A. Lorentz [28].

Appendix: a "rotlet analogue" of the basic theorem

In this Appendix I briefly show how the quantities defined by Eq. (65) behave in the limit as $X \to 1$. After the simple asymptotic property (66) has been derived for B_4, a "rotlet analogue" of the basic theorem is used to identify the logarithmic limiting behaviour of B_3.

The first derivation uses the idea that, when $| X - 1 |$ is very small, the integral expression (65) for B_4 is dominated by values of the integrand for small θ; say, with $0 < \theta < \Theta$ where Θ is defined as $| X - 1 |^{1/3}$. Indeed the rest of the range of integration (from Θ to ∞) makes a contribution to B_4 less in modulus than

$$\int_{\Theta}^{\infty} \frac{| X - 1 | \, \mathrm{d}\theta}{\alpha^3 \theta^3} = \frac{| X - 1 |}{2\alpha^3 \Theta^2} \quad \text{which} \quad \to 0 \text{ as } X \to 1. \tag{73}$$

But, for small enough θ, $\cos\theta$ can be replaced by $1 - \frac{1}{2}\theta^2$ so that the integral from 0 to Θ is estimated as

$$\int_0^{\Theta} \frac{(X-1)\mathrm{d}\theta}{[(\alpha^2 + \beta^2 X)\theta^2 + \beta^2 (X-1)^2]^{3/2}} = \frac{1}{\beta^2 (X-1)} \frac{\Theta}{[(\alpha^2 + \beta^2 X)\Theta^2 + \beta^2 (X-1)^2]^{1/2}}; \tag{74}$$

where, in the square bracket, the term $\beta^2 (X-1)^2$ is very small compared with the Θ^2 term of order $| X - 1 |^{2/3}$. Therefore, since $\alpha^2 + \beta^2 = 1$, expression (74) for the limiting behaviour of B_4 becomes

$$\frac{1}{\beta^2 (X-1)} [1 + \beta^2 (X-1) + O(| X - 1 |^{4/3})]^{-1/2}; \tag{75}$$

where, incidentally, the $O(| X - 1 |^{4/3})$ term incorporates too the error in replacing $\cos\theta$ by $1 - \frac{1}{2}\theta^2$. From Eq. (75), the asymptotic property (66) follows immediately.

A similar idea is used to investigate the relationship between B_3 for small $| X - 1 |$ and the quantity A_3 defined in Eq. (67). The aim is to find a small quantity ζ (which may depend on X) such that

$$[-\ln\zeta + A_3(\alpha)] - B_3(\alpha, X) \tag{76}$$

tends to zero as $X \to 1$.

Now, in the integral expressions (67) and (65) defining the two terms in (76), the difference of integrands is $2(1 - \cos\theta)$ times

$$[\alpha^2\theta^2 + 2\beta^2(1 - \cos\theta)]^{-3/2} - [\alpha^2\theta^2 + 2\beta^2 X(1 - \cos\theta) + \beta^2 (X-1)^2]^{-3/2}; \tag{77}$$

which, as $X \to 1$, tends uniformly to zero in the range $\Theta < \theta$ because $| X - 1 |$ is much smaller than θ^2. In the range $0 < \theta < \Theta$, moreover, $\cos\theta$ can be replaced by $1 - \frac{1}{2}\theta^2$ in both integrands. It follows that, in the limit as $X \to 1$, expression (76) becomes

$$\int_{\zeta}^{\Theta} \frac{\mathrm{d}\theta}{\theta} - \int_0^{\Theta} \frac{\theta^2 \mathrm{d}\theta}{[\theta^2 + \beta^2 (X-1)^2]^{3/2}} = \ln\frac{\Theta}{\zeta} - \sinh^{-1}\frac{\Theta}{\beta | X - 1 |} + \frac{\Theta}{[\Theta^2 + \beta^2 (X-1)^2]^{1/2}}; \tag{78}$$

which, since $\Theta = | X - 1 |^{1/3}$ is large compared with $\beta | X - 1 |$, can be rewritten as

$$\ln\frac{\Theta}{\zeta} - \ln\frac{2\Theta}{\beta | X - 1 |} + 1. \tag{79}$$

The aim of having it tend to zero as $X \to 1$ can be achieved, then, if

$$\zeta = \frac{1}{2}\mathrm{e}\beta \mid X - 1 \mid . \tag{80}$$

When this result (80) is applied on the surface of the cross-section, with radius a, of the helical sheath, the distance $R = bX$ from the axis of the helix must be given a value such that $\mid R - b \mid = a$ so that

$$\zeta = \frac{1}{2}\mathrm{e}kb \mid X - 1 \mid = \frac{1}{2}\mathrm{e}k \mid R - b \mid = \frac{1}{2}\mathrm{e}ka = k\delta\mathrm{e}^{1/2} = \epsilon\mathrm{e}^{1/2}, \tag{81}$$

in terms of $\epsilon = k\delta$ with $\delta = 0.5e^{1/2}a$, as defined between Eqs. (22) and (23) in Section 2 above. In order to specify motions of the cross-section surface, then, it is necessary to replace B_3 by

$$-\ln\zeta + A_3 = -\ln\epsilon - \frac{1}{2} + A_3; \tag{82}$$

which is precisely the conclusion stated (in turn) between Eqs. (67) and (68) in Section 4 above. Moreover, an exactly similar proof leads to just such an expression (but now involving A_1) for the value of B_1 on the surface.

References

1. J. Lighthill, Flagellar Hydrodynamics. *SIAM Review* 18 (1976) 161–230.
2. G.I. Taylor, Analysis of the swimming of microscopic organisms. *Proc. Roy. Soc. A* 209 (1951) 447–461.
3. G.I. Taylor, The action of waving cylindrical tails in propelling microscopic organisms. *Proc. Roy. Soc. A* 211 (1952) 225–239.
4. G.I. Taylor, Analysis of the swimming of long and narrow animals. *Proc. Roy. Soc. A* 214 (1952) 158–183.
5. J. Lighthill, Reinterpreting the basic theorem of flagellar hydrodynamics. *J. Eng. Maths.* 30 (1996) 25–34.
6. F.D. Warner and P. Satir, The substructure of ciliary microtubules. *J. Cell Sci.* 12 (1973) 313–326.
7. V.I. Chapman and D.J. Chapman, *The Algae*, 2nd Ed. New York: MacMillan (1973) 497 pp.
8. M. Parke and D.G. Rayns, Studies on Marine Flagellates VII. *Nephroselmis gilva* and some allied forms. *J. Marine Biol. Assoc. UK* 44 (1964) 209–217.
9. M.E.J. Holwill, Physical Aspects of Flagellar Movement. *Physiol. Rev.* 46 (1966) 696–785.
10. A.L. Lowndes, On flagellar movement in unicellular organisms. *Proc. Zool. Soc. London* 111 (1941) 111–134.
11. R.A. Lewin, Studies on the flagella of algae. I. General observations on *Chlamydomonas moewusii* Gerloff. *Biol. Bull.* 103 (1952) 74–79.
12. T.L. Jahn, W.M. Harrison and M. Landman, Mechanics of Locomotion in Flagellates. I. *Ceratium*. *J. Protozool.* 10 (1963) 358–363.
13. M.E.J. Holwill, The motion of *Euglena viridis*: the role of flagella. *J. Exp. Biol.* 44 (1966) 579–588.
14. E. Jawetz, J.L. Melnick and E.A. Adelberg, *Medical Microbiology*, 19th Ed. Englewood Cliffs, New Jersey: Prentice Hall (1991) 632 pp.
15. H.C. Berg, Dynamic properties of bacterial flagellar motors. *Nature* 249 (1974) 77–79.
16. B.L. Taylor and D.E. Koshland, Reversal of flagellar rotation in monotrichous and peritrichous bacteria: generation of changes in direction. *J. Bacteriol.* 119 (1974) 640–642.
17. A.J. Salle, *Fundamental Principles of Bacteriology*. New York: McGraw-Hill (1961) 812 pp.
18. R. Macnab and D. E. Koshland, Bacterial motility and chemotaxis: light-induced tumbling response and visualisation of individual flagella. *J. Molec. Biol.* 84 (1974) 399–406.
19. H.C. Berg and D.A. Brown, Chemotaxis in *Escherichia coli* analysed by three-dimensional tracking. *Nature* 239 (1972) 500–504.
20. V.V. Kingsley and J.F.M. Hoeniger, Growth, Structure and Classification of *Selenomonas*. *Bacteriol. Rev.* 37 (1973) 479–521.
21. A.T. Chwang, T.Y. Wu and H. Winet, Locomotion of spirilla. *Biophys. J.* 12 (1972) 1549–1561.
22. M. Ramia, Numerical model for the locomotion of spirilla. *Biophys. J.* 60 (1991) 1057–1058.
23. P. Metzner, Die Bewegung und Reizbeantwortung der bipolar begeisselten Spirillen. *Biol. Zentr.* 40 (1920) 49–87.

24. J.B. Baseman, The Spirochetes. In: B.D. Davis, R. Dulbecco, H.N. Eisen and H.S. Ginsberg (eds.) *Microbiology*, 4th Ed. Philadelphia: J.B. Lippincott (1990) pp. 673–685.
25. A.T. Chwang, H. Winet and T.Y. Wu, A theoretical mechanism of spirochetal locomotion. *J. Mechanochem. Cell Motility* 3 (1974) 69–76.
26. H.C. Berg, Bacterial movement. In: T.Y. Wu, C.J. Brokaw and C. Brennen (eds.) *Swimming and Flying in Nature*. New York: Plenum Press (1975) pp. 1–11.
27. R.L. Ricca, The effect of torsion on the motion of a helical vortex filament. *J. Fluid Mech.* 273 (1994) 241–259.
28. H.A. Lorentz. Eene algemeene stelling omtrent de beweging eener vloeistof met wrijving en eenige daaruit afgeleide gevolgen (A general theorem concerning the motion of a viscous fluid and a few consequences derived from it). *Versl. K. Acad. Wetensch. Amsterdam* 5 (1896) 168–175.